

STRUCTURE AND TOPOLOGY OF DUMORTIERITE AND DUMORTIERITE-LIKE MATERIALS

R. JAMES EVANS[§] AND LEE A. GROAT

*Department of Earth, Ocean and Atmospheric Sciences, University of British Columbia, 6339 Stores Road,
 Vancouver, British Columbia V6T 1Z4, Canada*

ABSTRACT

Dumortierite, *ca.* $(\text{Al}, \square)\text{Al}_6(\text{BO}_3)\text{Si}_3\text{O}_{13}(\text{O}, \text{OH})_2$, has a complex and unusual crystal structure that is shared by several minerals and an increasing number of synthetic materials, which we group together as dumortierite-like materials (DLMs). Dumortierite has a strongly pseudo-hexagonal orthorhombic structure based on rod-like double-chains of Al octahedra in a framework based on the {6·4·3·4} semi-regular planar tiling. The large hexagonal channels contain chains of face-sharing Al octahedra attached to the framework by rings of SiO_4 tetrahedra. Smaller triangular channels contain planar BO_3 groups, while in other materials the triangular channels are occupied by tetrahedral or pyramidal groups. Holtite and magnesioidumortierite are isostructural with dumortierite, while ellenbergerite, phosphoellenbergerite, ekatite, and the synthetic materials have very similar structures to dumortierite, but with hexagonal symmetry. These minerals and materials differ from one another in the identity of the metal cations occupying the framework and face-sharing chains, and in the tetrahedral, pyramidal, or triangular groups within the hexagonal and triangular channels. We write the following structure-generating function, which describes both topological and stoichiometric properties of DLMs:



where X is the face-sharing hexagonal channel octahedrally coordinated site, M is the framework octahedrally coordinated site, T^h and T' are three- to four-coordinate cation sites in the hexagonal and triangular channels, Φ is a four-coordinate anion site, Θ^h and Θ' are three-coordinate basal anion sites, and θ^h and θ' are one- to three-coordinate apical anion sites. We discuss various structural and crystal chemical properties of DLMs, illustrating their commonalities as variations on the theme described by the structure-generating function. We also discuss three closely related structures which involve modifications of different geometrical or topological aspects of the DLM structure: the structure of lyonsite and its synthetic analogues, the structure of satterlyite and holtedahllite, and the structure of the AB polytype of the cancrinite group of feldspathoids.

Keywords: structure topology, dumortierite, holtite, magnesioidumortierite, ellenbergerite, phosphoellenbergerite, ekatite, lyonsite, holtedahllite, satterlyite, cancrinite

INTRODUCTION

The crystal structure of dumortierite [*ca.* $(\text{Al}, \square)\text{Al}_6(\text{BO}_3)\text{Si}_3\text{O}_{13}(\text{O}, \text{OH})_2$] possesses several unusual features: chains of face-sharing octahedra, large hexagonal channels, and double-chains of edge-sharing octahedra. Several minerals and a growing number of synthetic compounds share the same or very similar structures.

Dumortierite is a widely distributed aluminum borosilicate (Grew 1996). Prior to determination of its structure, it was frequently classified with kyanite, andalusite, sillimanite, and mullite as a sillimanite-group mineral (Jeffery 1943) on the basis of its common physical resemblance, similar Al:Si:O proportions, and

tendency to decompose into mullite at high temperature. Claringbull & Hey (1958) determined the space group as *Pmcn* with $c \approx 4.7$, $a \approx 11.8$, and $b \approx 20.2$ Å. The crystal structure was first solved by Golovastikov (1965). Moore & Araki (1978b) did a detailed structural analysis which is the starting point of most contemporary crystal-chemical studies. They described Golovastikov's structure as "a design of great beauty and complexity" and remarked that

"A pronounced pseudo-hexagonal character was evinced among the intensity distributions and it is a credit to Golovastikov's imagination that he was able to decipher this unusually complicated structure based on Patterson projections."

[§] E-mail address: rjamesevans@gmail.com

Holtite [*ca.* (Al,Ta,Nb, \square)Al₆(BO₃)(Si,Sb,As)₃O₁₂(O,OH, \square)₃] and magnesioldumortierite [*ca.* (Mg,Ti, \square)Al₄(Al,Mg)₂(BO₃)Si₃O₁₂(OH,O)₃] were later found to be isostructural with dumortierite. Holtite is known from complex granitic pegmatites at four localities thus far: Greenbushes, Western Australia (Pryce 1971, Hoskins *et al.* 1989); Voron'i Tundry, Kola Peninsula, Russia (Voloshin *et al.* 1977); Szklary, Lower Silesia, Poland (Pieczka & Marszałek 1996, Pieczka *et al.* 2011); and Virocco, San Luis, Argentina (Galliski *et al.* 2012). Magnesioldumortierite has been found only in ultrahigh-pressure rocks of the western Alps (Chopin *et al.* 1995, Ferraris *et al.* 1995). Together, these three minerals comprise the dumortierite group of orthorhombic aluminum borosilicates. Dumortierite and holtite are distinctive among aluminosilicate minerals because they incorporate not only substantial amounts of the high field-strength lithophile elements Nb and Ta substituting for Al at octahedrally coordinated sites, but also significant quantities of the chalcophile elements As and Sb substituting for Si with a change of coordination (Groat *et al.* 2009, 2012).

Ellenbergerite [*ca.* (Mg,Ti,Zr, \square)Mg₃(Al,Mg)₃(Si,P)₄O₁₄(OH)₅], phosphoellenbergerite [*ca.* (Mg,Fe, \square)Mg₆(PO₄,PO₃OH,AsO₄)₃(PO₃OH,CO₃)(OH)₃], and ekatite [*ca.* (Fe³⁺,Fe²⁺,Zn)₆(AsO₃)₃(AsO₃,SiO₃OH)(OH)₃] have structures very similar to that of dumortierite, but with a hexagonal structure with space group *P6₃mc* or *P6₃*, depending on cation order. Ellenbergerite is known from the same high-pressure rocks in the western Alps as magnesioldumortierite (Chopin *et al.* 1986). Its phosphorus-rich, Si-free, endmember phosphoellenbergerite is known from the same source and from the magnesite-serpentine deposits in Modum, Norway (Raade *et al.* 1998). Ekatite is known only from the Tsumeb deposit in Namibia (Keller 2001). These minerals comprise the ellenbergerite group.

Several classes of synthetic compounds isostructural with hexagonal ellenbergerite have been produced via hydrothermal synthesis: the first-row divalent transition metal (TM) phosphites (Marcos *et al.* 1993b, 1993c, Atfield *et al.* 1994, Che *et al.* 2005, Gu *et al.* 2007, Ni *et al.* 2009, Jin *et al.* 2010, Liao & Ni 2010), metal pnictates (phosphates and arsenates) (Marcos *et al.* 1993a, 1995, Pizarro *et al.* 1993, Rojo *et al.* 2002, Hughes *et al.* 2003), the TM chalcogenites (selenites and tellurites) (Perez *et al.* 1976, Marcos *et al.* 1993a, Amorós *et al.* 1996), and the metal vanadates and sulfate-vanadates (Kato *et al.* 1998, Zhang *et al.* 1999, Đođević *et al.* 2008, Hu *et al.* 2008). Each of these compounds show crystal-chemical features seen in the dumortierite- and ellenbergerite-group minerals, as well as some novel features. They demonstrate that the underlying structure (which we shall refer to as the dumortierite structure, as it is the most common of these materials) is very adaptable, and is able to accommodate a wide variety of cations. We shall refer to a mineral or synthetic

compound isostructural to dumortierite or ellenbergerite as a dumortierite-like material (DLM).

In this paper, we examine the geometry and topology of the dumortierite structure in detail, and write a structure-generating function that describes both orthorhombic and hexagonal variants. We also discuss the related structures of lyonsite, satterlyite, and holte-dahlite, and the AB polytype of cancrinite, all of which share significant structural and topological similarities to dumortierite.

THE DUMORTIERITE STRUCTURE

Dumortierite and other DLMs may be described as having a (2+1)-dimensional structure, *i.e.*, a structure based on rod-like components that are assembled on a perpendicular two-dimensional net, such that many features of the structure can be understood by examining the net and the rod-like components separately. The net in the dumortierite structure is the semi-regular {6·4·3·4} tiling (Fig. 1), and the rod-like components are the double-chains of octahedra containing the Al₂, Al₃, and Al₄ sites (Fig. 2) and the face-sharing single chain of octahedra containing the Al₁ sites (Fig. 3), using the conventional site labels for the dumortierite group. The Al₄ and Al₂–Al₃ double-chains fit in the square regions of the net, sharing corners and forming small triangular and large hexagonal channels. The Al₁ chain of face-sharing octahedra floats in the center of the hexagonal channel, and is connected to the double-chains of octahedra by “pinwheels” of tetrahedral groups (SiO₄ in dumortierite), as in the “bracelet and pinwheel” structures described by Moore (1973). The small triangular channels are occupied by BO₃ triangles in the dumortierite group, and by various tetrahedral or pyramidal groups in other DLMs. The complete structure is shown in Figure 1B. The double-chains of octahedra thus form a framework to which the other elements are attached; dumortierite and other DLMs can be appropriately described as metal oxides with decorations. This framework of rod-like components is responsible for the needle-like morphology of many DLMs.

Two kinds of double-chains of octahedra form the framework of the orthorhombic dumortierite structure. Both are constructed from a pair of zigzag single chains of edge-sharing octahedra. In the Al₄ double-chain (top of Fig. 2), one of these single chains is stacked on top of its mirror image in the plane of connection perpendicular to [100], resulting in a chain of face-sharing dimers of octahedra. Each Al₄ octahedron shares a face with one other Al₄ octahedron, edges with two other Al₄ octahedra, and corners with two Al₄ octahedra in the same double-chain, as well as corners with three tetrahedra in the hexagonal channel, one group in the triangular channel, and one Al₂ octahedron in a neighboring Al₂–Al₃ double-chain. This kind of face-sharing

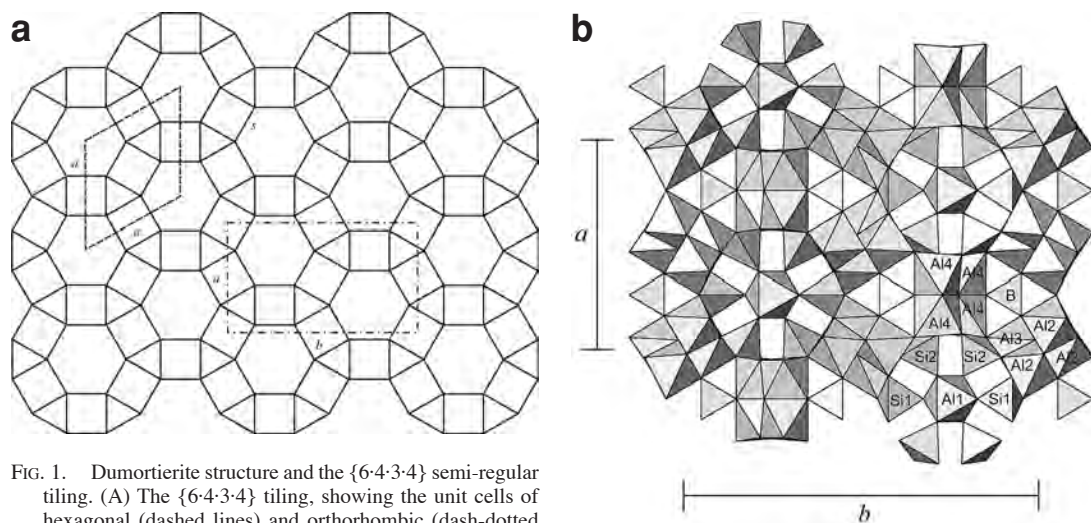


FIG. 1. Dumortierite structure and the $\{6\cdot4\cdot3\cdot4\}$ semi-regular tiling. (A) The $\{6\cdot4\cdot3\cdot4\}$ tiling, showing the unit cells of hexagonal (dashed lines) and orthorhombic (dash-dotted lines) DLMs; all edges have length s . (B) Crystal structure of dumortierite viewed down the c -axis (space group $Pm\bar{c}n$).

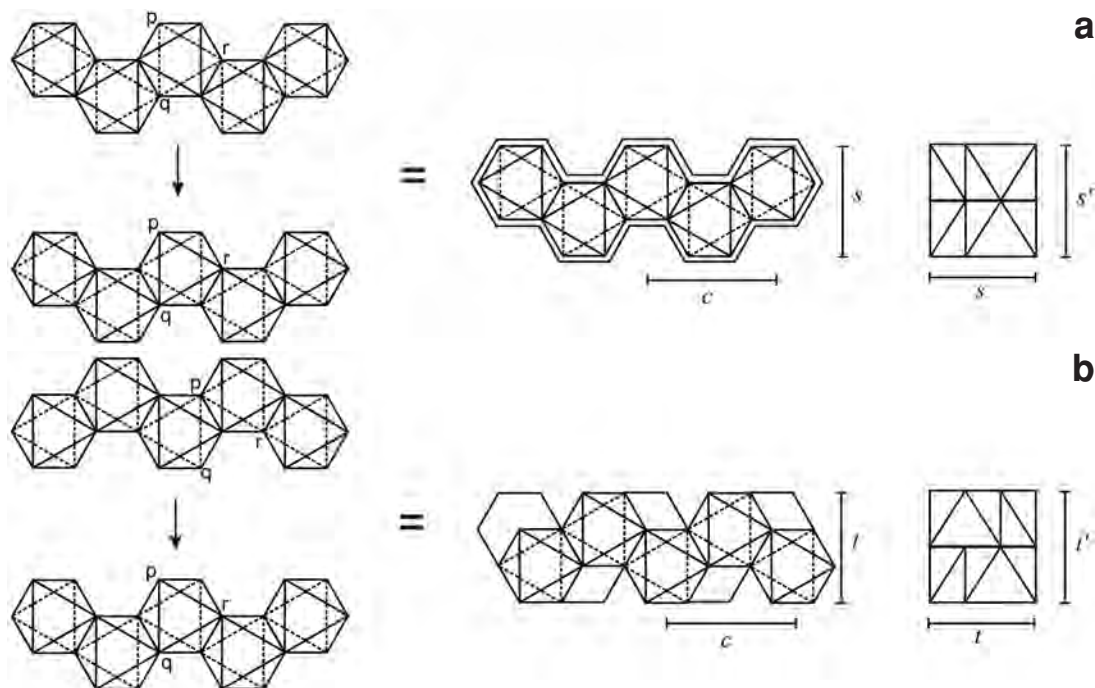


FIG. 2. Construction of the (A) M^H (Al4) and (B) M^C (Al2–Al3) double-chains of octahedra in the dumortierite structure. In the complete double chains, the points labeled p , q , r on the upper single chains are joined to the corresponding p , q , r points on the lower single chains. As a result, octahedra share faces as well as edges in the M^H (Al4) chains, but only edges in the M^C (Al2–Al3) chains. Here s is the width of the double-chain, s' is the height of the double-chain, and c is the unit cell parameter.

double-chain also occurs in the related structures of the minerals holtedahllite (Raade & Mladeck 1979, Rømming & Raade 1989) and satterlyite (Mandarino *et al.* 1978, Kolitsch *et al.* 2002), which have other features in common with the dumortierite structure, as discussed below.

The Al2–Al3 double-chain (bottom of Fig. 2) is geometrically similar to the Al4 double-chain, but topologically it is quite different with regards to its bond connectivity. In the Al2–Al3 double-chain, one single chain is shifted with respect to a second so that the two chains are connected by edge sharing only. Alexander *et al.* (1986) described the doubling of the Al2–Al3 chains as an inversion through the point ($\frac{1}{2}$, $\frac{1}{2}$, $\frac{1}{2}$). The resulting double-chain is a cubic close-packed arrangement, whereas the Al4 double-chain is hexagonally close-packed (Moore & Araki 1978b). Each Al2 (Al3) octahedron shares edges with one other Al2 (Al3) octahedron and three Al3 (Al2) octahedra in the same double-chain, as well as corners with three tetrahedra in the hexagonal channel, one group in the triangular channel, and one Al4 (Al3) octahedron in a neighboring Al4 (Al2–Al3) double-chain. This type of cubic close-packed double-chain also occurs in the structure of the mineral angelellite (Moore & Araki 1978a), $(\text{Fe}^{3+}_2\text{O})_2\text{O}(\text{AsO}_4)_2$.

The orthorhombic dumortierite-group minerals contain Al2–Al3 and Al4 double-chains in a 2:1 ratio, whereas the hexagonal ellenbergerite-group minerals and synthetic DLMs contain only Al4-type double-chains. No hexagonal DLM has been reported to contain only Al2–Al3-type chains, and as discussed below, it is not possible to build a dumortierite-like structure only

with Al2–Al3-type chains. In dumortierite, the Al2, Al3, and Al4 octahedra are very similar in size (that is, in volume and mean bond-length) and are distorted from octahedral symmetry in similar ways. As the two types of double-chain are based on different kinds of anion close-packing, there seems to be no spatial advantage of one type of double-chain over the other. In dumortierite, the minimum Al^{3+} – Al^{3+} distance in the Al4 double-chains is 2.56 Å across shared faces, whereas in the Al2–Al3 double-chains, the minimum distance is 2.86 Å. All hexagonal DLMs observed and synthesized thus far are dominated by divalent cations, as are holtedahllite (a magnesium phosphate) and satterlyite (its Fe^{2+} analogue), or by divalent and trivalent cations in equal proportions. In all three orthorhombic DLMs, the octahedrally coordinated sites in the double-chains are strictly dominated by Al^{3+} , including magnesiodumortierite, which has small but significant Mg^{2+} substitution at the Al4 site; similarly, the octahedrally coordinated sites in angelellite predominantly contain Fe^{3+} . It seems likely that trivalent cations prefer the Al2–Al3-type double-chains because the longer minimum cation-cation distance reduces electrostatic repulsion. Dumortierite, therefore, is orthorhombic because it contains (mostly) aluminum at its octahedrally coordinated framework double-chain sites. Ellenbergerite and ekatite contain mixed divalent and trivalent cations in their Al4-type double-chains in roughly equal proportions (Mg^{2+} or Al^{3+} in the former and Fe^{2+} , Zn^{2+} , or Fe^{3+} in the latter); a sufficiently large excess of trivalent cations may drive these minerals to an orthorhombic structure isostructural with dumortierite.

Calculation of unit-cell parameters

The symmetry of the dumortierite-group minerals is commonly given as both $Pm\bar{c}n$ (with $c < a < b$) and the equivalent $Pnma$ (with $a < b < c$). In this work, we use the $Pm\bar{c}n$ setting for orthorhombic DLMs for two reasons: (1) for continuity with the hexagonal DLMs, which use the same labeling for equivalent **a** and **c** axes and their associated unit-cell parameters (*i.e.*, $c_{\text{orth}} \rightarrow c_{\text{hex}}$, $a_{\text{orth}} \rightarrow a_{\text{hex}}$, $b_{\text{orth}} \rightarrow \sqrt{3} a_{\text{hex}}$), and (2) in terms of xyz coordinates, the chains of octahedra and open channels now extend parallel to the **z** axis (instead of the **x** axis), whereas the underlying {6·4·3·4} tiling lies in the xy -plane (instead of the yz -plane), and it is thus more natural to speak of directions ‘up’ or ‘down’ the channels or chains.

The semi-regular tiling {6·4·3·4} is shown in Figure 1A. The same set of polygons meet at every vertex in the same order: hexagon, square, triangle, hexagon; hence the labeling of the vertex and thus the tiling, {6·4·3·4}. Where every edge has the same length (s), the tiling has plane-group symmetry $p6mm$ with a unit cell as shown by the dashed line in Figure 1A. Stretching or compression parallel to one of the three vertex-to-vertex diameters of the hexagon results in a distorted ortho-

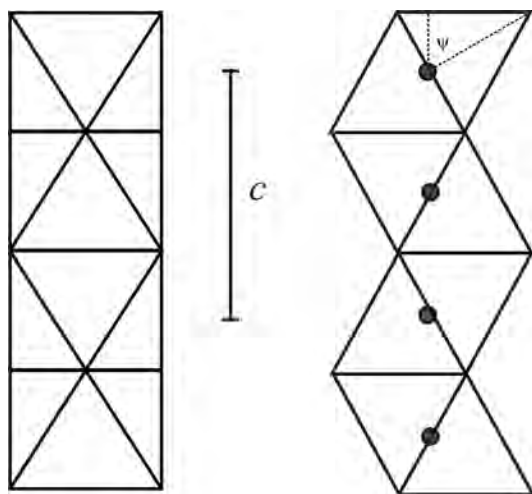


FIG. 3. X (Al1) chain of face-sharing octahedra viewed along the **a** (left) and **b** (right) axes. Circles represent the cation position. The flattening angle ψ is labeled.

rhombic tiling with plane-group symmetry $c2mm$ and a unit cell as shown by the dash-dotted line in Figure 1A. The contents of the unit cells have a tile stoichiometry of

$$\{6\}\{4\}_3\{3\}_2$$

where $\{n\}$ is an n -sided regular polygon, with $Z = 1$ and 2 for the hexagonal and orthorhombic unit cells, respectively. If we let $\{nlm\}$ indicate an edge where polygons $\{n\}$ and $\{m\}$ meet, each formula unit also contains six $\{3|4\}$ and six $\{4|6\}$ edges, as well as six $\{6\cdot4\cdot3\cdot4\}$ vertices. The tiling adheres to the version of Euler's formula valid for graphs drawn on the surface of torus, Faces + Vertices – Edges = 0. (Because opposite edges of the unit cell are equal, the unit cell of a 2D tiling is topologically equivalent to a torus.)

In the undistorted hexagonally symmetric tiling, $a = (1 + \sqrt{3})s$ and $b = (3 + \sqrt{3})s$, so that $b/a = \sqrt{3} \approx 1.732$. Hexagonal symmetry is preserved if every square in the $\{6\cdot4\cdot3\cdot4\}$ tiling is replaced by a rectangle with sides (s, s'), such that the hexagons are of side s and the triangles of side s' , resulting in

$$a = \sqrt{3}s + s', b = 3s + \sqrt{3}s'. \quad (1)$$

If two squares on opposite sides of the hexagon are smaller than the other four squares it can be shown that b/a is reduced below $\sqrt{3}$. In dumortierite, Al4 octahedra are smaller in volume than Al2–Al3 octahedra by about 1.3%, and $b/a = 1.714$, about 1% less than $\sqrt{3}$ (Evans *et al.* 2012).

As a first approximation, we will assume that the double-chains of octahedra are built of identical regular octahedra with the cation M at the center, with an M–O bond length d (the actual Al2, Al3, and Al4 octahedra have significant distortions). Such an octahedron will have edge-length $e = \sqrt{2}d$ and height, which we define as the distance between centers of opposite faces, $h = 2d/\sqrt{3}$. Both Al4 and Al2–Al3 chains (Fig. 2) then have a height of

$$s' = 2h = \frac{4\sqrt{3}}{3}d \quad (2)$$

and width

$$s = \frac{3}{2}e = \frac{3\sqrt{2}}{2}d \quad (3)$$

Equations 2 and 3 give $s/s' = 3\sqrt{6}/8 \approx 0.92$, so the double-chains of octahedra do not deviate from the square profiles shown in Figure 1A by more than 8%. The a and b unit-cell parameters from equations 1, 2, and 3 are

$$a = \left(\frac{3\sqrt{6}}{2} + \frac{4\sqrt{3}}{3} \right) d, b = \sqrt{3}a \quad (4)$$

Similarly, the c unit-cell parameter can be also be calculated from the geometry of the double-chains. The

center-to-center distance between edge-sharing regular octahedra is equal to e , and so

$$c = \sqrt{3}e = \sqrt{6}d \quad (5)$$

and

$$\frac{a}{c} = \frac{3}{2} + \frac{2\sqrt{2}}{3} \approx 2.443 \quad (6)$$

Taking an $^{VI}\text{Al}^{III}\text{O}$ bond length of 1.90 Å (Shannon 1976) in equations 4 and 5 gives $a = 11.37$, $b = 19.69$, and $c = 4.65$ Å. For a geometric first-principles calculation, this compares reasonably well with the actual unit cell of dumortierite: $a = 11.79$, $b = 20.19$, and $c = 4.69$ Å for dumortierite without major substitutions (Evans *et al.* 2012).

The face-sharing chain of Al1 octahedra (Fig. 3) offers another route for calculating the c unit-cell parameter. Consider an octahedron distorted into a trigonal antiprism, either stretched or flattened along an axis normal to one pair of opposite faces such that those faces remain equilateral triangles and all six M–O distances remain equal to d . Face-sharing octahedra are often stretched in this way, whereas edge-sharing octahedra in sheets are flattened, in both cases to reduce repulsion between cations. The height of the distorted octahedron is

$$h_{\text{Al1}} = 2d \cos\psi \quad (7)$$

where ψ is the angle between the distortion axis and the M–O bonds. In a regular octahedron, $\psi = \tan^{-1}\sqrt{2} \approx 54.74^\circ$, whereas $\psi < 54.74^\circ$ for stretched and $\psi > 54.74^\circ$ for flattened octahedra. From Figure 3 and equation 7,

$$c = 2h_{\text{Al1}} = 4d \cos\psi \quad (8)$$

Equating equations 5 and 8 gives $\cos\psi = \sqrt{6}/4$ or $\psi \approx 52.24^\circ$. The actual Al1 octahedron in dumortierite is not flattened uniformly; ψ differs for the Al1–O2 and Al1–O7 bonds, and Al1 is not at the center of the octahedron. However, the average ψ for Al1 in dumortierite is 52.17° (Evans *et al.* 2012). The main determinant of distortion of the Al1 octahedron is thus a match between the Al1 chain and the framework of double-chains of octahedra.

The near-hexagonality of the orthorhombic dumortierite structure leads to the twinning commonly seen in dumortierite and holtite crystals, with the twin components related by 120° rotations about an axis parallel to c . An example is the (As,Sb)-bearing blue dumortierite from Lake Uvil'dy, Russia, which shows reticular pseudomorph twinning based on a pseudohexagonal lattice with $c \sim c_{\text{dum}}$, $a \sim 2a_{\text{dum}}$, $\gamma \sim 119.4^\circ$ (Groat *et al.* 2012). The underlying structure can be modeled based on (slightly) orthorhombic nets as in Figure 1A, rotated 120° about the near-threefold axes

extending down the hexagonal or triangular channels and stacked on top of one another. A consequence of this stacking is the creation of faults or defects in the double-chains of octahedra, where Al4-type chains join Al2–Al3-type chains.

STRUCTURE-GENERATING FUNCTION

By examining the local connectivity of bonds and how components are assembled in the {6·4·3·4} net, we can construct a structure-generating function for the dumortierite structure. The structure-generating function is a powerful generalized formula that describes both stoichiometric (*i.e.*, composition) and topological (*i.e.*, structure and bond connectivity) information for a class of minerals or materials with common features (Hawthorne 2010). In our case, we can write a structure-generating function that describes both hexagonal and orthorhombic DLMs.

Following Hawthorne (2010), we represent generalized cation sites by uppercase Latin letters and generalized anion sites by Greek letters. We use Θ for a 3-coordinate anion and Φ for a 4-coordinate anion. We represent anions with variable occupancy and coordination that occupy the apex of a tetrahedron or pyramid with a lowercase θ .

We start with the structure of dumortierite itself. Table 1 lists the 18 sites in dumortierite and their linkages. Inspection of the table shows that O10 and O11 are Φ -type anions and O1, O3–O6, O8, and O9 are Θ -type anions. Note that O10 is coordinated only by Al4 and O11 only by Al2 and Al3, so that the 4-coordinate anions are contained entirely within their respective double-chains. Of the 3-coordinate anions, O1 and O3–O6 coordinate the tetrahedrally coordinated sites in the hexagonal channel (Si1 and Si2), whereas O8 and O9 coordinate the cation in the triangular channel (B); we thus designate O1 and O3–O6 as Θ^h and O8 and O9 as Θ^t .

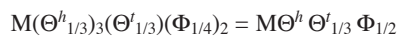
Atoms O2 and O7 are also 3-coordinate if the Al1 site is fully occupied, but their role in the structure is quite different from that of the other anions. They are the only anions that are not part of the double-chain framework, and where the Al1 site is vacant (which it commonly is), their coordination drops to 2. In holtite and (As,Sb)-substituted dumortierite, the O2 and O7 sites are often vacant. We therefore consider them to be θ -type anions and label them θ^h .

Finally, we consider the possibility of replacing B in the triangular channel with a 4-coordinated cation. This is the situation in all DLMs, excluding the dumortierite-group minerals, including ellenbergerite, which has Si or P in the triangular channel. This adds an apical site Θ^t inside the triangular channel, which may be 1-coordinated, 2-coordinated if shared between adjacent tetrahedral cations in the channel, or vacant as in dumortierite.

With the anions properly labeled, we can construct the local environment of the cations. Consider a closed

surface centered on each cation that passes through each of its coordinating anions; for anions that are shared by N cations, each surface apportions $1/N$ of the anion to each cation. We consider the region bounded by the surface as the local environment of the central cation. Summing the contents of all such bounded regions in the unit cell gives some multiple of the chemical formula.

From Table 1, we see that each of the double-chain sites Al2, Al3, and Al4 are bonded to three Θ^h , one Θ^t , and two Φ anions. In this sense, the Al4 and Al2–Al3 chains are topologically equivalent. Letting M be a general octahedrally coordinated cation site in the double-chains, the M coordination octahedron can be written as



where the fractional subscripts indicate the sharing of anions between cations. In both types of double-chains of octahedra there are four complete octahedra per repeat distance along the c -axis (see Fig. 2), so in the {6·4·3·4} net

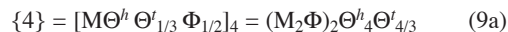


TABLE 1. SITES IN DUMORTIERITE AND THEIR CONNECTIVITY

Label	Site	Bonded To
X	Al1	O2 × 2, O7 × 4
M ^C *	Al2 Al3	O1, O3, O5, O9, O11 × 2 O3, O5, O6, O9, O11 × 2
M ^H *	Al4	O4 × 2, O6, O8, O10 × 2
T ^h	Si1 Si2	O2, O1, O3 × 2 O7, O4, O5, O6
T ^t	B	O8, O9 × 2
θ^h	O2 O7	Si1, Al1 × 2 Si2, Al1 × 2
Θ^h	O1 O3 O4 O5 O6	Si1, Al2 × 2 Si1, Al2, Al3 Si2, Al4 × 2 Si2, Al2, Al3 Si2, Al3, Al4
Θ^t	O8 O9	B, Al4, Al4 B, Al2, Al3
$\Phi^{H\uparrow}$	O10	Al4 × 4
$\Phi^{C\uparrow}$	O11	Al2 × 2, Al3 × 2

* M^H, M^C are both type M in expression 10a.

† $\Phi^{H\uparrow}$, $\Phi^{C\uparrow}$ are both type Φ in expression 10a.

For now, we continue to neglect the difference between the Al2–Al3 and Al4 types of double-chains of octahedra. When it becomes necessary to distinguish them, we shall write M^H , Φ^H for sites in the hexagonal-close packed Al4-type and M^C , Φ^C for sites in the cubic-close packed Al2–Al3-type.

The tetrahedrally coordinated sites in the hexagonal channel, Si1 and Si2, are coordinated by three Θ^h and one θ^h anion each, giving

$$T^h(\Theta^h_{1/3})_3\theta^h_{1/3} = T^h\Theta^h\theta^h_{1/3}$$

for each tetrahedron, where T^h is the general tetrahedrally coordinated site. The octahedrally coordinated site in the hexagonal channel, Al1, is coordinated by six θ^h anions. Labeling the generalized site X, we have

$$X(\theta^h_{1/3})_6 = X\theta^h_2$$

For each repeat distance along the **c**-axis, there are two complete X octahedra and two rings of three T^h tetrahedra, and so in the {6·4·3·4} net,

$$\{6\} = [X\theta^h_2] [T^h\Theta^h\theta^h_{1/3}] [X\theta^h_2] [T^h\Theta^h\theta^h_{1/3}]_3 = [XT^h_3\Theta^h_3\theta^h_3]_2 \quad (9b)$$

Finally, the triangular channel cation site B is coordinated by three Θ^t anions and one θ^t anion (where applicable). Calling the general triangular channel site T^t , the local environment is

$$T^t(\Theta^t_{1/3})_3\theta^t = T^t\Theta^t\theta^t = \{3\} \quad (9c)$$

as there is only one T^t site per repeat distance along the **c**-axis.

Combining equations 9a-c with the {6·4·3·4} tile stoichiometry,

$$\{6\}\{4\}_3\{3\}_2 = [XT^h_3\Theta^h_3\theta^h_3]_2 [(M_2\Phi)_2\Theta^h_4\Theta^t_{4/3}]_3 [T^t\Theta^t\theta^t]_2 = 2[X(M_2\Phi)_3(T^h\Theta^h_3\theta^h)_3(T^t\Theta^t\theta^t)]$$

Dropping the factor of 2, this gives us the generalized structure-generating function for DLMs,

$$X(M_2\Phi)_3(T^h\Theta^h_3\theta^h)_3(T^t\Theta^t\theta^t) \quad (10a)$$

To emphasize the distinction between the orthorhombic and hexagonal versions of the structure, we reintroduce the two types of double-chains of octahedra:

$$X(M^H_2\Phi^H)_{3-m}(M^C_2\Phi^C)_m(T^h\Theta^h_3\theta^h)_3(T^t\Theta^t\theta^t) \quad (10b)$$

where $M^H_2\Phi^H$ now indicates the Al4-type double-chain, $M^C_2\Phi^C$ indicates the Al2–Al3-type double-chain, and $m = 2$ for the orthorhombic and 0 for the hexagonal structures. The expression compartmentalizes the chemically distinct structural elements - the tetrahedral/pyramidal/

triangular groups $T^h\Theta^h_3\theta^h$ and $T^t\Theta^t_3\theta^t$, the double-chain elements $M^H_2\Phi^H$ and $M^C_2\Phi^C$, and the highly variable octahedrally coordinated hexagonal channel site X. Expressions 10a or 10b can now be applied to any material, natural or synthetic, with the dumortierite structure.

THE HEXAGONAL VERSUS ORTHORHOMBIC STRUCTURES

Despite broad similarities between the hexagonal and orthorhombic variants of the dumortierite structure, there are significant differences apart from symmetry and the presence of M^C double-chains.

As discussed by Ferraris *et al.* (1995), the (2+1)-dimensional structure can be broken into component slabs perpendicular to the **a** direction. This is shown in Figure 4A for the hexagonal structure and Figure 4B for the orthorhombic structure. In the underlying {6·4·3·4} net, these slabs correspond to rows of squares and hexagons alternating with rows of triangles and squares. In Figure 4, we shift the $T^t\Theta^t_3\theta^t$ groups from the second slab to the first so that the second slab consists of only corner-sharing double-chains of octahedra, but this is arbitrary.

The hexagonal structure is built of two types of slabs, labeled 1 and 2 in Figure 4A. The type-1 slabs consist of M^H double-chains of octahedra (light and dark green in Fig. 4), $T^t\Theta^t_3\theta^t$ groups (blue), and the hexagonal channels (yellow), whereas type-2 slabs consist of corner-sharing M^H chains. The $T^h\Theta^h_3\theta^h$ tetrahedra in the hexagonal channels are oriented the same way in all the type-1 slabs (indicated by a circle with a central dot, denoting an arrow pointing out of the page), as are the M^H chains. The point-group symmetry allows the complete structure to be rotated by multiples of 120° and decomposed into the same type of slabs in the same way.

The orthorhombic structure is composed of four types of slab (Fig. 4B), but with the second two related to the first two by a simple transformation. The first slab is the same type-1 as in the hexagonal structure. The second slab, labeled type-3, consists of chains of edge-sharing M^C octahedra (pink and light blue) and is analogous to the type-2 slabs in the hexagonal structure. The third and fourth slabs, labeled types- $\bar{1}$ and $\bar{3}$, are inverted slabs of types-1 and 3; as a consequence, the hexagonal channels in type- $\bar{1}$ slabs are oriented oppositely to those in type-1 (indicated by the crossed circle, denoting an arrow pointing into the page; an alternative way of decomposing the orthorhombic structure into only two kinds of slabs can be obtained by rotating the structure by 120°, as shown in the deposited Supplemental Figure S1; available from the Depository of Unpublished Data on the Mineralogical Association of Canada website, document Dumortierite CM50_1197.)

The alternating orientations of slabs 1,3 and $\bar{1},\bar{3}$ in the orthorhombic structure show that transforming an orthorhombic DLM such as dumortierite into a hexag-

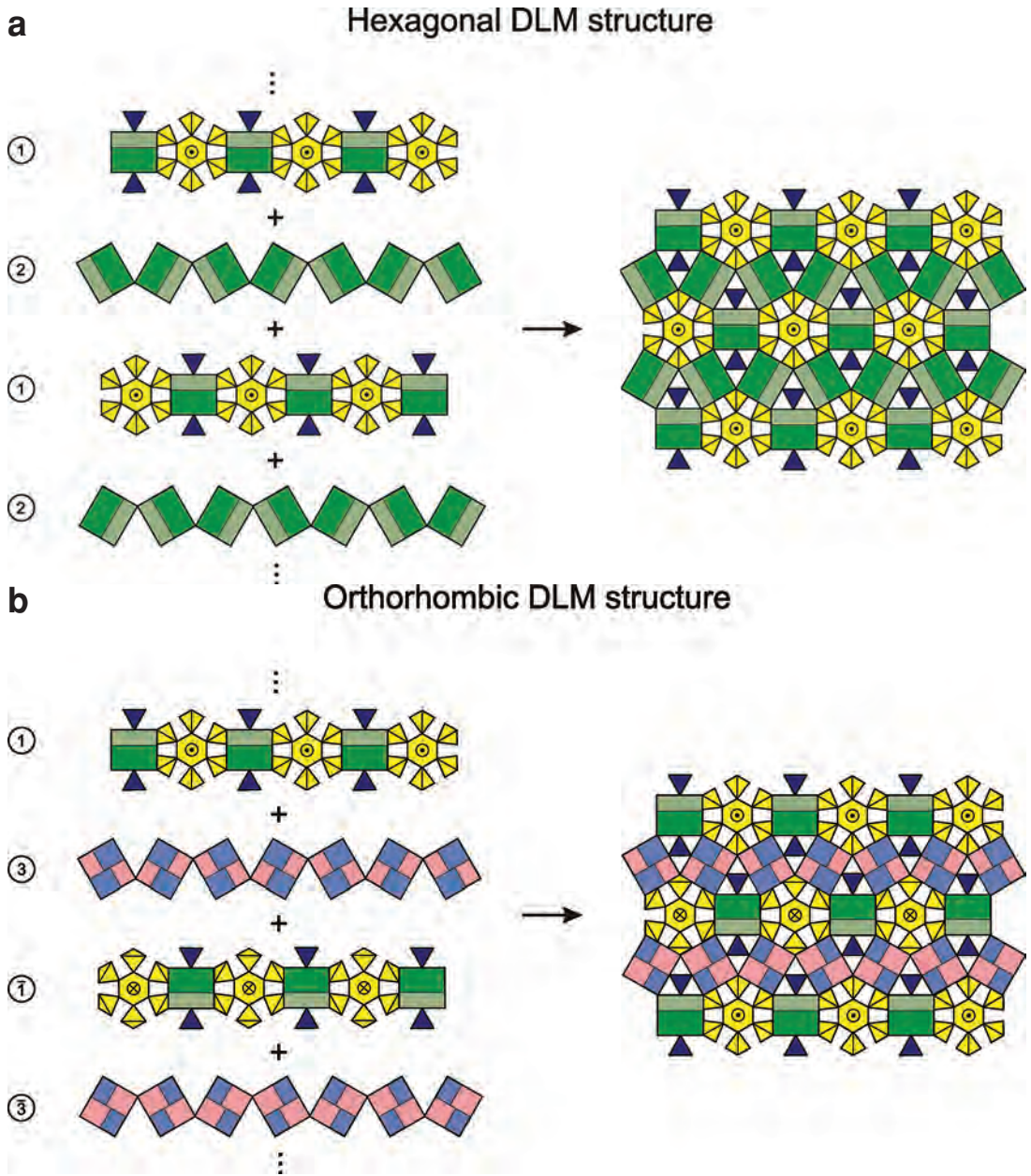


FIG. 4. Decompositions of the hexagonal (A) and orthorhombic (B) dumortierite-like structure, highlighting differences between them, after Ferraris *et al.* (1995). The hexagonal structure is built of alternating slabs in the bc -plane of type 1 and 2; the orthorhombic structure is built of layered slabs of type 1, 3, 1, and 3, where type x is related to type x by an inversion. The uppermost dimer of M^H octahedra is shown as a dark green rectangle within the larger M^H chain rectangle, with the lower dimer just behind shown as lighter green. In the M^C double-chains, Al2 octahedra are pink and Al3 octahedra pale blue; upper octahedra are represented by full rectangles, while lower octahedra behind are represented by partial rectangles. The $T\Theta'_3\theta'$ groups are shown as blue triangles. The contents of the hexagonal channel are shown in yellow. The orientation of the tetrahedra in the hexagonal channels is shown by either a circle with a dot, denoting an arrow pointing out of the page, or a circle with a cross, denoting an arrow pointing into the page.

onal analogue is not simply a matter of transforming M^C chains into M^H chains, but also involves reorientation of half the crystal structure. From these considerations, Ferraris *et al.* (1995) concluded that the transformation of dumortierite into a hexagonal phase as suggested by Moore & Araki (1978b) would be difficult.

The double-chains in Figure 4 are necessarily flattened into square two-dimensional profiles; upper and lower octahedra or dimers of octahedra are indicated graphically as described in the figure caption. It can be seen that both the M^H and M^C double-chains adhere to the following matching rules: upper octahedra can only share corners with upper octahedra, and lower octahedra can only share corners with lower octahedra. By inspection, it is clear that there is no way to surround the triangular channel with M^C chains alone such that these matching rules are followed, hence a

dumortierite-like structure with M^C chains but no M^H chains is impossible.

REVIEW OF DUMORTIERITE-LIKE MATERIALS

With the structure-generating function in place, much of the crystal chemistry of DLMs can be described with reference to the identity of the various terms in expression 10. Having a common description of the structure allows us to directly compare chemically and crystallographically distinct materials. We now review the known materials with the dumortierite structure with reference to the structure-generating function. Previously, Zubkova *et al.* (2006) compared several chemically and structurally distinct DLMs, but here we include several additional members and go into greater detail. A summary of known DLMs is given in Table 2.

TABLE 2. DUMORTIERITE-LIKE MATERIALS, $X(M^H_2\Phi^H)_{3-m}(M^C_2\Phi^C)_m(T^h\Theta^h_3\theta^h)_3(T^t\Theta^t_3\theta^t)$

Material	Space Group	X	$M^H_2\Phi^H$	$M^C_2\Phi^C$	$T^h\Theta^h_3\theta^h$	$T^t\Theta^t_3\theta^t$
Dumortierite	<i>Pmcn</i>	Al, □, Fe, Ti, Mg, ...	Al ₂ (O,OH)	Al ₂ O	SiO ₄ ⁴⁻ , SiO ₃ OH ³⁻ , AlO ₄ ⁵⁻ , AsO ₃ ³⁻ , SbO ₃ ³⁻ , PO ₄ ³⁻	BO ₃ ³⁻
Holtite	<i>Pmcn</i>	Al, □, Ta, Nb, Ti, Fe, Mg, ...	Al ₂ (O,OH)	Al ₂ O	SiO ₄ ⁴⁻ , AsO ₃ ³⁻ , SbO ₃ ³⁻ , SiO ₃ OH ³⁻ , AlO ₄ ⁵⁻ , PO ₄ ³⁻	BO ₃ ³⁻
Magnesian-dumortierite	<i>Pmcn</i>	Mg, □, Ti, Fe	(Al, Mg) ₂ OH	Al ₂ O	SiO ₄ ⁴⁻ , SiO ₃ OH ³⁻ , PO ₄ ³⁻	BO ₃ ³⁻
Ellenbergerite	<i>P6₃</i> (ordered) or <i>P6₃mc</i> (disordered)	Mg, Ti, □, Zr, Fe ²⁺ , ...	Mg ₂ OH + Al ₂ OH or (Mg, Al) ₂ OH		SiO ₄ ⁴⁻ , PO ₄ ³⁻ , SiO ₃ OH ³⁻ , PO ₃ OH ²⁻	SiO ₄ ⁴⁻ , PO ₄ ³⁻ , SiO ₃ OH ³⁻ , PO ₃ OH ²⁻
Phospho-ellenbergerite	<i>P6₃mc</i>	Mg, □, Ti, Zr, Fe ²⁺ , Ca...	Mg ₂ OH		PO ₄ ³⁻ , PO ₃ OH ²⁻ , AsO ₄ ³⁻ , SO ₄ ²⁻ , SiO ₄ ⁴⁻	PO ₃ OH ²⁻ , CO ₃ ²⁻ , SiO ₄ ⁴⁻
Ekatite	<i>P6₃mc</i>	□	(Fe ³⁺ , Fe ²⁺ , Zn) ₂ OH		AsO ₃ ³⁻	AsO ₃ ³⁻ , SiO ₃ OH ³⁻
TM* Phosphites	<i>P6₃mc</i>	□	(M _{11/12} □ _{1/12}) ₂ OH for M = Co ²⁺ , Ni ²⁺ , Zn ²⁺ , Fe ²⁺ , Mn ²⁺		HPO ₃ ²⁻	HPO ₃ ²⁻
Metal Phosphates	<i>P6₃mc</i>	□ _{1-x/2} M _{x/2} for M = Co ²⁺ , Ni ²⁺ , Mg	M ₂ OH for M = Co ²⁺ , Ni ²⁺ , (Mg, Ni ²⁺)		TO ₃ OH ²⁻ , TO ₄ ³⁻ for T = P ⁵⁺ , As ⁵⁺	TO ₃ OH ²⁻ , TO ₄ ³⁻ for T = P ⁵⁺ , As ⁵⁺
TM* Chalcogenites	<i>P6₃mc</i>	OH ⁻ , F ⁻	M ₂ OH for M = Co ²⁺ , Ni ²⁺		TO ₃ ²⁻ for T = Se ⁴⁺ , Te ⁴⁺	TO ₃ ²⁻ for T = Se ⁴⁺ , Te ⁴⁺
Zn sulfate-vanadate	<i>P6₃mc</i>	Zn ²⁺ , □?	Zn ₂ OH		VO ₄ ³⁻ , VO ₃ OH ²⁻ ?	SO ₄ ²⁻ , SO ₃ OH ⁻ ?
Metal vanadates	<i>P6₃mc</i>	M, □ for M = Mn ³⁺ , Mg	M ₂ OH for M = Mn ²⁺ , Mg		VO ₄ ³⁻ , VO ₃ OH ²⁻	VO ₄ ³⁻ , VO ₃ OH ²⁻ , V ₂ O ₇ ⁴⁻ , V ₂ O ₆ OH ³⁻

*TM: transition metal

Dumortierite, holtite, and magnesiodumortierite

There are 18 crystallographically distinct sites in dumortierite, but many play the same roles topologically in the structure and so are considered to be equivalent in terms of the structure-generating function. For example, whereas the Si1 and Si2 sites are crystallographically distinct, they are both considered to be T^h sites. Similarly, Al2 and Al3 are both considered M^C sites, and O1 and O3–O6 are all Θ^h sites.

In the dumortierite-group minerals, both M^H (Al4) and M^C (Al2–Al3) double-chains of octahedra are present, so $m = 2$ in expression 10b. In dumortierite, sites in the double-chains of octahedra are predominantly occupied by Al^{3+} , so M^C and M^H are equal to Al^{3+} . The O11 (Φ^C) site seems invariably to be occupied by oxygen, so $M^C_2\Phi^C$ is equal to Al_2O . Bond-valence calculations for all three dumortierite-group minerals (Alexander *et al.* 1986, Ferraris *et al.* 1995, Fuchs *et al.* 2005, Kazantsev *et al.* 2005) show that the O10 (Φ^H) site has a low incident valence and is partially occupied by OH, so that $M^H_2\Phi^H$ is equal to $Al_2(O,OH)$. As discussed by Alexander *et al.* (1986) and Moore & Araki (1978b), the Φ^H anion is coplanar with its four bonded M^H cations, and repulsion between the cations elongates two of the four M^H – Φ^H bonds. This leads to the low incident valence and makes Φ^H a receptive site for OH⁻ or F⁻. This is common in hexagonal DLMs, as shown below. In dumortierite group minerals these OH groups balance charges for divalent cations substituting for Al^{3+} at the M sites. The H at Φ^H forms a hydrogen bond with one of the Θ^l anions (O8 in dumortierite) (Ferraris *et al.* 1995).

Like the M sites, the octahedrally coordinated site Al1 in the hexagonal channel is generally dominated by Al^{3+} , but it is also, on average, between 10% and 25% vacant (Moore & Araki 1978b, Alexander *et al.* 1986, Fuchs *et al.* 2005, Evans *et al.* 2012); thus X is equal to (Al, \square) . Large anisotropic-displacement parameters along the **c**-axis indicate that in some cases, the Al1 site in dumortierite is split (Evans *et al.* 2012, Groat *et al.* 2012), with Al^{3+} atoms relaxing toward adjacent vacancies so as to increase the minimum Al–Al distance in the hexagonal channel. In some cases, this produces order in individual channels of trimers of occupied Al1 octahedra separated by vacancies as found by Evans *et al.* (2012). In other cases, additional substitutions lead to disordered sequences of dimers, trimers, and longer sequences (Groat *et al.* 2012).

Vacancies at Al1 are charge-compensated by replacement of O by OH somewhere in the structure. In dumortierite, this is considered to occur primarily at the O2 and O7 positions (Moore & Araki 1978b, Alexander *et al.* 1986, Werding & Schreyer 1990, Ferraris *et al.* 1995, Cempírek & Novák 2005, Fuchs *et al.* 2005, Evans *et al.* 2012) adjacent to vacant Al1 sites; thus $\theta^h = (O, OH)$. *Ab initio* electronic structure calculations (Evans *et al.* 2012) suggest that H at O2 and O7 form

hydrogen bonds with under-bonded O^{2-} at other O2, O7 sites associated with the vacant Al1 octahedron.

Anion sites other than O2, O7, and O10 are most likely O^{2-} only; Ferraris *et al.* (1995) suggested OH at the O1 or O9 sites, but there is little supporting evidence. Endmember dumortierite has Si^{4+} at all Si1 and Si2 sites, so $T^h\Theta^h_3\theta^h$ is primarily $SiO_3(O,OH)$. The only cation that has been reported at the cation site in the triangular channel in dumortierite, holtite, or magnesiodumortierite to date is B^{3+} , so $T^l\Theta^l_3\theta^l$ is equal to BO_3^{3-} (with $\theta^l = \square$). The full formula for endmember dumortierite written in the format of expression 10b is thus



Common substituents for Al^{3+} at the octahedrally coordinated X, M^C , and M^H sites include Ti^{4+} , Fe^{3+} , Fe^{2+} , and Mg^{2+} (Claringbull & Hey 1958, Beukes *et al.* 1987, Taner & Martin 1993, Platonov *et al.* 2000, Choo & Kim 2003, Farges *et al.* 2004, Cempírek & Novák 2005, Fuchs *et al.* 2005, Mahapatra & Chakrabarty 2011, Pieczka *et al.* 2011, Evans *et al.* 2012). The larger and more flexible octahedra coordinating the X site can also accommodate Nb^{5+} and Ta^{5+} . Small amounts of phosphorus (typically ~ 0.1 wt. % P_2O_5 or less) are commonly detected in dumortierite, presumably as PO_4^{3-} at $T^h\Theta^h_3\theta^h$. The total content of octahedrally coordinated cations in dumortierite frequently exceeds the theoretical maximum of 7 *apfu*, with a closely corresponding deficit of (T^h -type) tetrahedrally coordinated cations below 3 *apfu*, strongly suggesting small amounts of Al^{3+} at the T^h sites (*cf.* Ferraris *et al.* 1995, Chopin *et al.* 1995, Evans *et al.* 2012, Groat *et al.* 2012). In synthesizing dumortierite, Werding & Schreyer (1990) found greater amounts of tetrahedrally coordinated Al^{3+} at low pressures than at high pressures.

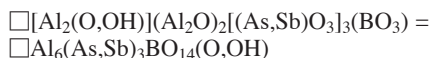
The material that gives rose quartz its color is closely related to dumortierite: it forms fibrous nanoinclusions, ranging in width from 0.1 to 0.5 μm (Applin & Hicks 1987, Goreva *et al.* 2001). Goreva *et al.* (2001) found the FTIR and Raman spectra of the fibers to be similar to those of dumortierite with some slight differences in the 1000 and 350–600 cm^{-1} regions. Ma *et al.* (2002) reported that selected-area electron-diffraction (SAED) patterns and high-resolution transmission-electron microscope (HRTEM) images show that the fibers have a superstructure with a doubled periodicity along the **a**- and **b**-axes, giving cell parameters $a = 2a_{dum} = 23.6 \text{ \AA}$, $b = 2b_{dum} = 40.5 \text{ \AA}$, and $c = c_{dum} = 4.7 \text{ \AA}$. Computer simulations suggest that periodic arrangements of two different X-site occupancies give rise to the superstructure; one type of X site is occupied mainly by Al^{3+} , whereas the other is dominated by Ti and Fe. Analytical electron microscopy (AEM) showed that the fibers contain significant amounts of Ti (0.15–0.25 *apfu*) and Fe (0.09–0.15 *apfu*) substituting for Al. The color of rose quartz likely originates from Fe-Ti

charge-transfer along the X sites in the fibers (Goreva *et al.* 2001, Platonov *et al.* 2000).

Holtite (Pryce 1971) differs from dumortierite in incorporating substantial amounts of Ta⁵⁺ and Nb⁵⁺ at the X sites and (AsO₃³⁻, SbO₃³⁻) as T^hΘ^h₃Θ^h groups. The apical Θ^h anions (O2 and O7 sites) are replaced by lone pairs of electrons on the As³⁺ or Sb³⁺ cations (Kazantsev *et al.* 2005); this creates linked X-site vacancies as coordinating anion sites are vacant. The (As,Sb) sites are slightly displaced from the Si positions to accommodate the longer bond-lengths.

None of the four constituents that distinguish holtite from dumortierite is dominant at a specific crystallographic site, *i.e.*, Si is dominant over Sb³⁺ and As³⁺ at the two tetrahedrally coordinated sites and Al is dominant over Ta and Nb at the Al1 site in both minerals. Significant As³⁺ and Sb³⁺ have been reported in dumortierite from various localities (Groat *et al.* 2001, Borghi *et al.* 2004, Vaggelli *et al.* 2004, Cempírek & Novák 2004, Cempírek *et al.* 2010, Pieczka *et al.* 2011, Groat *et al.* 2012, Galliski *et al.* 2012). Pieczka *et al.* (2011) described a dumortierite-like mineral from the Szklary pegmatite, Poland, with As + Sb > Si and negligible Ta, Nb, and Ti, occurring as a few tiny inclusions (≤ 20 μm across) in quartz. Tantalum is dominant over Nb at the X site in most holtite (Groat *et al.* 2009), but Pieczka *et al.* (2011) have reported Nb-dominant holtite from Szklary. Cempírek *et al.* (2010) and Pieczka *et al.* (2011) have also reported holtite-like compositions with substantial (As³⁺, Sb³⁺) and Ti⁴⁺ (~0.25 *apfu* or greater) instead of (Ta⁵⁺, Nb⁵⁺) as the high-valence cation at the X site. The holtite- and dumortierite-like material from Szklary is highly zoned, and these various compositions occur in close proximity. The several generations of dumortierite-holtite found at the Virorco locality (Galliski *et al.* 2012) display a full range of compositions including high-(Ta,Nb) with high-(As,Sb) (holtite), low-(Ta,Nb) with high-(As,Sb), high-(Ta,Nb) with low-(As,Sb); and low-(Ta,Nb) with low(As,Sb) (traditional dumortierite).

These results show that not only does there exist a compositional continuum between dumortierite and holtite, but that this continuum comprises multiple endmembers, including Si-dominant dumortierite-holtite analogues where Ta⁵⁺, Nb⁵⁺, or Ti⁴⁺ are dominant at the X site, as well as the material with total replacement of SiO₄⁴⁻ by (As,Sb)O₃³⁻:



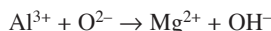
This latter material features a completely vacant X site and hence an empty hexagonal channel. Whereas ekatite and certain synthetic hexagonal DLMs possess empty hexagonal channels (see below), it is uncertain whether these hypothetical Si-free dumortierite-like endmembers would be stable. Full characterization of the dumortierite-holtite system requires a precise definition of each of these endmembers and a consistent

nomenclature, specifically, clarification of what qualifies an orthorhombic Al-dominated DLM as ‘holtite’.

Magnesioldumortierite (Ferraris *et al.* 1995, Chopin *et al.* 1995) is the Mg-analogue of dumortierite. Here, Mg²⁺ is dominant at the X site (over vacancies, Ti⁴⁺, Fe²⁺, and Fe³⁺); up to 0.40 Mg has been observed at the M^H (Al4) site (Chopin *et al.* 1995), although Al³⁺ is still dominant at the latter. The Mg²⁺ replaces Al³⁺ in the dumortierite structure via the mechanisms



and



with the latter mechanism favored at high pressures (Chopin *et al.* 1995). Ferraris *et al.* (1995) located OH at the Φ^H (O10) site on a difference Fourier map, and bond-valence calculations indicate that Φ^H is completely occupied by OH, with approximately another 0.5 H at each Θ^h (O2 and O7) site. Other sites in magnesioldumortierite are the same as in dumortierite.

Figure 5 shows a plot of unit-cell parameters *b* versus *a* for dumortierite (30 natural samples, 21 synthetic), holtite (9 natural samples), and magnesioldumortierite (1 natural sample), together with the hexagonal ideal of *b* = √3*a* (equations 1, 4). Nearly all measured unit-cell parameters fall below this line of hexagonality; the average *b/a* for natural dumortierite is 1.714(5) and for holtite is 1.713(2), where figures in brackets indicate standard deviations; for the single measured sample of magnesioldumortierite (Ferraris *et al.* 1995), *b/a* = 1.713. Points for naturally occurring dumortierite cluster mostly in the lower left of the diagram (*a* ~ 11.78–11.83 Å, *b* ~ 20.17–20.28 Å), whereas the points for holtite are spread across the upper right following a similar trend (*a* ~ 11.87–11.98 Å, *b* ~ 20.30–20.57 Å); magnesioldumortierite falls in the holtite range. In the synthetic dumortierite prepared by Werding & Schreyer (1990) (white circles in Fig. 5), in which Al₂O₃, SiO₂, B₂O₃, and H₂O are the only components, higher synthesis pressures resulted in greater *b* and smaller *a* values, as well as lower analytical Al/Si ratios and lower amounts of tetrahedrally coordinated Al.

Ellenbergerite, phosphoellenbergerite, and ekatite

The ellenbergerite group minerals are the only naturally occurring DLMs known with hexagonal symmetry; they possess only M^H-type and no M^C-type double-chains, such that *m* = 0 in the structure-generating function (expression 10b).

Ellenbergerite (Chopin *et al.* 1986) is a Mg-dominated silicate-phosphate found as inclusions in pyrope porphyroblasts from the southern Dora-Maira massif in the western Alps, Italy. Its general formula is

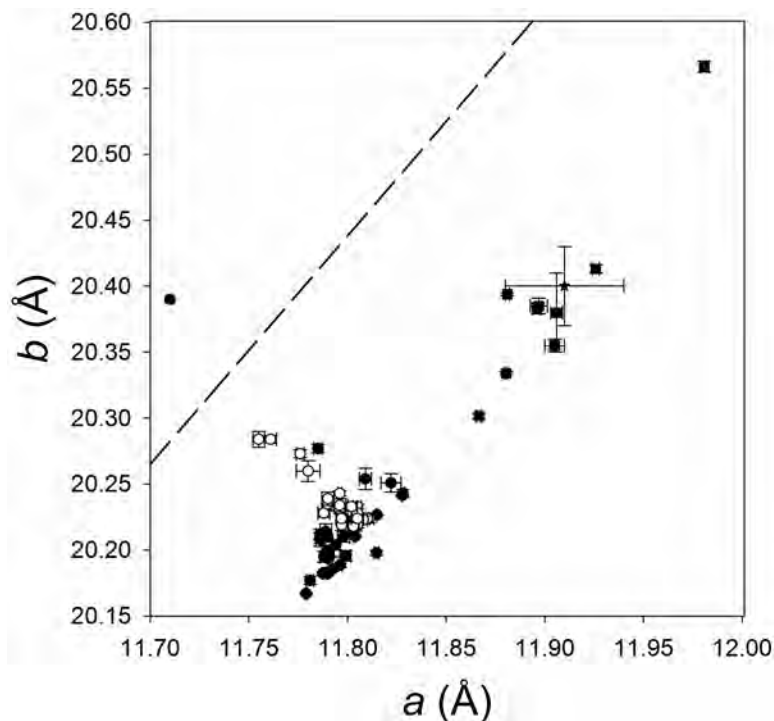
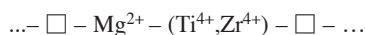


FIG. 5. Unit-cell parameters b versus a (space group $Pm\bar{c}n$) for dumortierite group minerals. The black circles represent naturally-occurring dumortierite [4 unpublished data, 12 from Alexander *et al.* (1986), 4 from Groat *et al.* (2012), 2 from Fuchs *et al.* (2005), 2 from Evans *et al.* (2012), and one each from Moore & Araki (1978b), Beukes *et al.* (1987), Taner & Martin (1993), Choo & Kim (2001), Cempírek & Novák (2005), and Mahapatra & Chakrabarty (2011)]; white circles, synthetic dumortierite [21 from Werding & Schreyer (1990)]; black squares, holtite [one unpublished datum, 4 from Groat *et al.* (2009), and one each from Pryce (1971), Hoskins *et al.* (1989), Kazantsev *et al.* (2006), and Zubkova *et al.* (2006)]; the black star represents magnesiodumortierite [from Ferraris *et al.* (1995)]; the dashed line is $b = \sqrt{3}a$.



The hexagonal channel site, X, is occupied primarily by Mg along with the tetravalent cations Ti and Zr, vacancies and small amounts of Fe^{2+} (Chopin *et al.* 1986). The substitution $\text{Ti}^{4+} \leftrightarrow \text{Zr}^{4+}$ results in color variations from purple to colorless. Cations appear to be ordered along the hexagonal channel in the following fashion:



(Chopin & Langer 1988, Comodi & Zanazzi 1993a); coloration occurs due to Fe^{2+} - Ti^{4+} (pink to purple) and Fe^{2+} - Fe^{3+} (blue) charge transfer between adjacent X sites (Chopin & Langer 1988, Chopin *et al.* 2009), similar to the case of dumortierite (Platonov *et al.* 2000).

The $\text{T}^h\Theta^h_3\theta^h$ groups in the hexagonal channel and $\text{T}'\Theta'_3\theta'$ groups in the triangular channel can be silicate or phosphate groups. Chopin *et al.* (1986) proposed a silicate endmember $(\text{Mg}_{1/3}\text{Ti}_{1/3}\square_{1/3})\text{Mg}_3\text{Al}_3\text{Si}_4\text{O}_{14}(\text{OH})_5$ with the main substitution mechanism a mixture of $\text{VIAl}^{3+} + \text{IVSi}^{4+} \leftrightarrow \text{VIMg}^{2+} + \text{IVP}^{5+}$ (~80%) and $\text{VIAl}^{3+} + \text{IVSi}^{4+} \leftrightarrow \text{VIAl}^{3+} + \text{IVP}^{5+}$ (~20%). The former alone can account for replacement of a maximum of 3 Si *pfu*. Brunet & Schaller (1996) suggest that $\text{Si}^{4+} + \text{H}^+ \leftrightarrow \text{P}^{5+}$ is also active.

Near the silicate endmember composition, Al and Mg are ordered at distinct sites in the M^H double-chain, lowering the space group symmetry to $P6_3$. With a higher P content, Al and Mg are disordered, with only one M^H site, and the space group is $P6_3mc$.

Mineral compositions near the phosphate endmember are designated phosphoellenbergerite (Brunet &

Schaller 1996, Raade *et al.* 1998). Chopin *et al.* (1986) reported compositions with up to 16 wt.% P₂O₅ (> 2 *apfu*). Zoned crystallites with Si-rich cores and P-rich rims or vice versa are common (Chopin & Sobolev 1995, Brunet *et al.* 1998). Endmember phosphoellenbergerite was later synthesized with stoichiometry (Mg_{1-x}□_x)(Mg₂OH)₃(PO₄)_{3-2x}(PO₃OH)_{1+2x}, *x* = 0.1 (Brunet & Schaller 1996, Brunet *et al.* 1998).

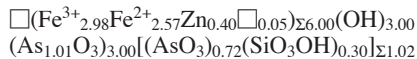
Phosphoellenbergerite is also found at the Tingelstadjern serpentinite-magnesite deposit, Modum, Norway as inclusions in heunite (Raade *et al.* 1998), with the stoichiometry (Mg,Fe,□)(Mg₂OH)₃(PO₄, PO₃OH, AsO₄)₃(PO₃OH,CO₃). As well as phosphate, substantial carbonate substitutes for TⁱΘⁱ3θⁱ groups in the triangular channel (2.75 wt.%) via PO₃OH²⁻ ↔ CO₃²⁻, whereas the T^hΘ^h3θ^h groups in the hexagonal channel may also be AsO₄³⁻, SO₄²⁻, or SiO₄⁴⁻ via the substitutions PO₄³⁻ ↔ AsO₄³⁻ and 2PO₄³⁻ ↔ SO₄²⁻ + SiO₄⁴⁻ (Raade *et al.* 1998).

Silicon-bearing ellenbergerite and phosphoellenbergerite form a complete solid-solution series (Chopin & Sobolev 1995). Phosphoellenbergerite, a high-pressure phase, breaks down into polymorphs of Mg₃(PO₄)₂ and Mg₂(PO₄)OH (the latter include holtehdahlite, see below) below 8.5 kbar at 650 °C, below 22.5 kbar at 900 °C, and below 30 kbar at 975 °C (Brunet *et al.* 1998). It has a greater field of stability than Si endmember ellenbergerite, which is only stable above 27 kbar and 725 °C (Chopin *et al.* 1992). The difference in stability between the Si and P endmembers and their complete solid solution has led to Si/P ratios in ellenbergerite being suggested as a geobarometer (Chopin & Sobolev 1995).

As in dumortierite, OH⁻ is located in the double-chains at Φ^H and in the hexagonal channels at θ^h, as well as at θⁱ in the triangular channels. The total OH content depends on P content and the occupancy of the X site. Chopin *et al.* (1986) found 7-8 wt.% H₂O in ellenbergerite, corresponding to approximately 5 OH *pfu*, and found via bond-valence calculations that both OH⁻ and O²⁻ are present at Φ^H and θ^h. Bond-valence calculations for phosphoellenbergerite suggest that Φ^H and θⁱ are entirely OH⁻ (Brunet & Scaller 1996, Raade *et al.* 1998, Zubkhova *et al.* 2007), and the presence of OH⁻ at these sites was confirmed via infrared and NMR spectroscopy (Brunet & Schaller 1996). The H atom in the trigonal channel at θⁱ does not sit on the threefold axis down the center of the channel, but in a disordered position off the axis (Brunet & Schaller 1996).

Ferraris *et al.* (1995) reported that magnesiodumortierite and ellenbergerite are found in contact at the Dora-Maira massif, with the ellenbergerite being nearly boron-free. This suggests that Al³⁺ and B³⁺ prefer the orthorhombic structure whereas Mg²⁺ and P⁵⁺ prefer the hexagonal structure.

Ekatite (Keller 2001), a mixed-valence iron arsenite-silicate found at Tsumeb, Namibia, has the empirical formula



(rescaled from Keller 2001 for *Z* = 2) with space group *P6₃mc*. All T^hΘ^h3θ^h groups are AsO₃³⁻, such that the θ^h sites are occupied by the As³⁺ lone-pair electrons, and there are no coordinating anions for the X site in the hexagonal channel; thus X is completely vacant. Ekatite is therefore similar to the hypothetical Si-free dumortierite-holtite endmember. Arsenite also dominates TⁱΘⁱ3θⁱ groups in the triangular channel, with a minority occupied by SiO₃OH³⁻ groups. As in phosphoellenbergerite, H atoms in the triangular channel are at disordered positions off the threefold axis. Hydrogen was located on Φ^H and θⁱ on difference Fourier maps, and bond-valence calculations suggest that both sites are entirely filled by OH⁻. Stoichiometry and bond valences indicate an average M^H valence of 2.5, which with chemical analyses leads to the given occupancy. There was no evidence of ellenbergerite-like order in the M^H chains.

Synthesis of DLMs

Two of the six mineral DLMs have been synthesized. Synthesis of dumortierite was first reported by Ono (1981) and Werding & Schreyer (1983), and Werding & Schreyer (1990) did extensive experiments under various synthesis conditions. Endmember phosphoellenbergerite was synthesized by Beller (1987), Brunet & Schaller (1996), and Brunet *et al.* (1998).

The first new synthetic DLMs reported were Ni and Co hydroxytellurites by Perez *et al.* (1976); several other types have been produced since then. Synthetic DLMs are grown hydrothermally in closed vessels at various pressures (0.4 to 30 kbar) and temperatures (160 to 1100 °C). All are hexagonal with space group *P6₃mc*, with divalent cations dominating the octahedrally coordinated framework (M^H) sites. None have yet been synthesized containing Al³⁺, borate or silicate groups.

TM phosphites

One of the most studied class of synthetic DLMs are the transition metal (TM) phosphites with stoichiometry M₁₁(HPO₃)₈(OH)₆. These have been synthesized with M = Co²⁺ (Marcos *et al.* 1993b, Che *et al.* 2005, Ni *et al.* 2009), Ni²⁺ (Marcos *et al.* 1993b, Gu *et al.* 2007, Ni *et al.* 2009, Liao & Ni 2010), Zn²⁺ (Marcos *et al.* 1993c), Fe²⁺ (Attfield *et al.* 1994), and Mn²⁺ (Attfield *et al.* 1994, Jin *et al.* 2010).

In terms of the structure-generating function (expression 10), the general formula for the TM phosphites can be written as



with $x = 1/12$. Both $T'\Theta'_3\theta'$ and $T^h\Theta^h_3\theta^h$ are HPO_3^{2-} groups, tetrahedral groups with oxygen at the three basal vertices and a hydride anion, H^- , at the apex, so that $\Theta' = O^{2-}$ and $\theta' = H^-$. With the hydrogen atoms of the phosphite group pointing into the hexagonal channel, the X site is vacant.

Phosphite tetrahedra in the triangular channel show various orientations depending on the M^H cation. In hexagonal DLMs, the $T^h\Theta^h_3\theta^h$ tetrahedra in the hexagonal channel point in a uniform direction, so that we may describe the $3\Theta^h$ triangular base of a tetrahedron as pointing up the c-axis as in Figure 6A. The $T'\Theta'_3\theta'$ tetrahedra in the triangular channel may point either in the same or opposite directions. Ellenbergerite-group minerals seem to prefer $T'\Theta'_3\theta'$ pointing up, *i.e.*, in the same direction as the $T^h\Theta^h_3\theta^h$ tetrahedra; ellenbergerite, phosphoellenbergerite, and ekatite all have $T'\Theta'_3\theta'$ groups that point up (carbonate groups in phosphoellenbergerite are planar with $\theta' = \square$). In the TM

phosphites, phosphite groups in the triangular channel point up for the Zn^{2+} , Fe^{2+} , and Mn^{2+} compounds (Marcos *et al.* 1993c, Attfield *et al.* 1994). The Ni^{2+} compound, however, has phosphite groups in the triangular channel that point down, *i.e.*, against the direction of the $T^h\Theta^h_3\theta^h$ tetrahedra (Marcos *et al.* 1993b). The Co^{2+} compound has split T' and θ' sites separated by 0.87 and 1.4 Å, respectively, so that approximately 80% of the phosphite groups point down and 20% point up (Marcos *et al.* 1993b). It is not clear why phosphite prefers to point down in these two compounds but up in most of the others, and whether this is controlled strictly by the identity of the M cation or is affected by synthesis conditions.

Note that there is no standard setting for the dumortierite or ellenbergerite group minerals with regards to which direction along the c-axis is "up", *e.g.*, the reduced unit-cell coordinates used for dumortierite by Moore & Araki (1978b) and for ekatite by Keller (2001) have the T^h tetrahedra pointing in the positive c direction, whereas those for ellenbergerite used by Chopin *et al.* (1986) and for phosphoellenbergerite by Raade *et al.* (1998) have the T^h tetrahedra pointing in the negative c direction.

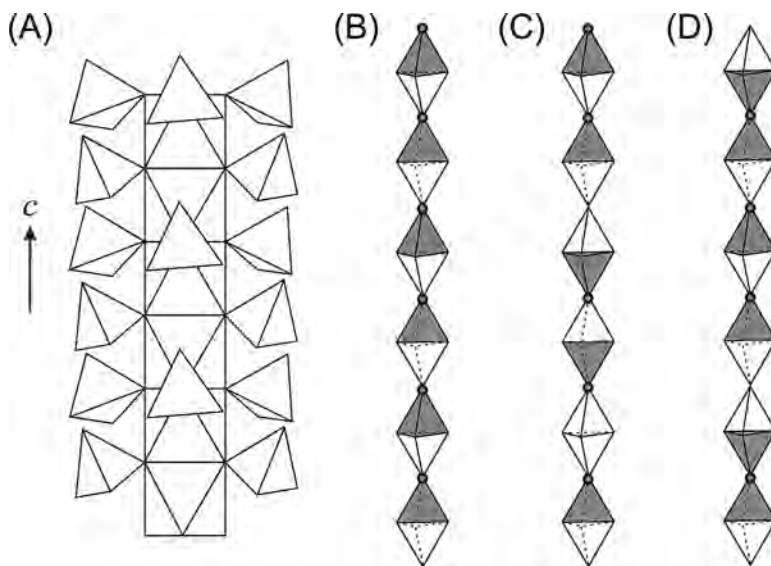


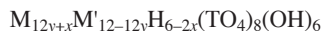
FIG. 6. Orientation of the tetrahedral groups. (A) Section of the hexagonal channel showing the tetrahedral $T^h\Theta^h_3\theta^h$ groups. The tetrahedral groups point in a uniform direction (defined here as the positive direction of the c-axis), and the $T'\Theta'_3\theta'$ groups in the triangular channel may point either up or down with respect to that direction. (B), (C), and (D) Possible distribution of tetrahedra in the triangular channels. Shaded tetrahedra indicate occupied T' sites and filled circles indicate occupied θ' sites. (B) Completely ordered triangular channel with all $T'\Theta'_3\theta'$ groups pointing up. (C) Disordered triangular channel with no apex sharing; θ' occupancy is equal to total T' (upward- and downward-pointing) occupancy. (D) Disordered triangular channel with apex sharing; θ' occupancy is equal to upward-pointing T' occupancy.

Structure refinement of single-crystal (Marcos *et al.* 1993c) and powder (Marcos *et al.* 1993b) X-ray diffraction data show that the occupancy of the M^H site is very close to the $11/12$ predicted by the ideal stoichiometry, with no evidence of order among the vacancies, although Marcos *et al.* (1993c) did detect some evidence of a split site 0.4 \AA from the regular cation site, presumably due to relaxation near a vacancy. With the M^H cation the only variable, the unit-cell parameters show a simple linear dependence on cation size (Fig. 7). The M^H cation also controls the color of the compounds: translucent to white for Zn^{2+} , pink to violet for Co^{2+} ,

grey or light green to green for Ni^{2+} , colorless for Fe^{2+} , and white to pink for Mn^{2+} .

Metal pnictates

Several compounds have been synthesized with a general stoichiometry described, following the formulae used by Pizarro *et al.* (1993) and Rojo *et al.* (2002), by



where $M, M' = Co^{2+}, Ni^{2+}, Mg^{2+}$ and $T = P^{5+}$ or As^{5+} with $0 \leq x \leq 2$ and $0 \leq y \leq 1$ (y undefined when $M =$

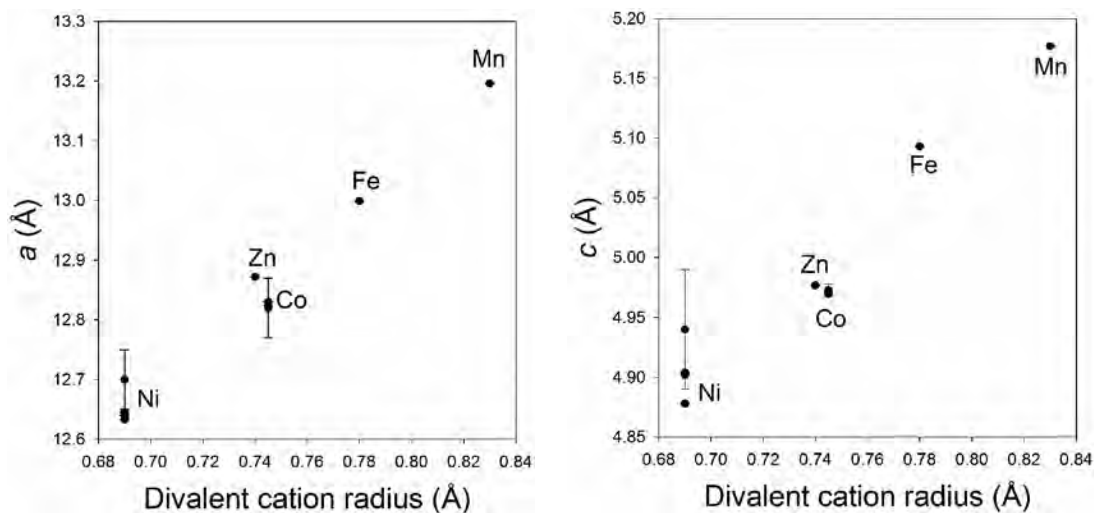


FIG. 7. Unit-cell parameters of TM phosphites (M^H cations labeled) versus cation radius (Shannon 1976). (A) a parameter, (B) c parameter. Data from Marcos *et al.* (1993b), Marcos *et al.* (1993c), Atfield *et al.* (1994), Che *et al.* (2005), Gu *et al.* (2007), Ni *et al.* (2009), and Liao & Ni (2010).

TABLE 3. SYNTHETIC METAL PNICTATES, $M_{12y+x}M'_{12-12y}H_{6-2x}(TO_4)_8(OH)_6$

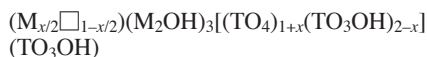
M	M'	T	x	y	c (Å)	a (Å)	Ref.
Co	Co	P	1.22		5.031	12.580	1, 2
Co	Co	As	1.32		5.092	12.828	3
Ni	Ni	P	0.78			not given	1
Ni	Ni	P	0.76		4.953	12.470	2
Ni	Ni	As	1.33		5.031	12.695	4
Ni	Ni	As	1.16		5.032	12.702	4
Ni	Ni	As	0.96		4.997	12.702	3
Ni	Ni	As	0.78		5.026	12.678	2
Mg	Ni	P	0.00	$2/3$	4.974	12.419	5
Mg	Ni	As	1.50	0.76	5.062	12.715	5
Mg	Mg	P	1.80		5.003-5.008	12.431-12.437	6*

References: [1] Pizarro *et al.* (1993), [2] Marcos *et al.* (1993a), [3] Hughes *et al.* (2003), [4] Marcos *et al.* (1995), [5] Rojo *et al.* (2002), [6] Brunet and Schaller (1996), Brunet *et al.* (1998).

*endmember phosphoellenbergerite.

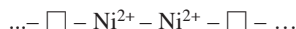
M'). The endmember phosphoellenbergerite described by Brunet & Schaller (1996) and Brunet *et al.* (1998) fits this category, with $M = M' = \text{Mg}^{2+}$, $T = \text{P}^{5+}$ and $x = 1.8$, so these compounds might be considered further extrapolations of ellenbergerite. Various compositions with $M = M' = \text{Co}^{2+}$, Ni^{2+} were synthesized by Pizarro *et al.* (1993), Marcos *et al.* (1993a, 1995), and Hughes *et al.* (2003). Rojo *et al.* (2002) synthesized mixed compositions with $M = \text{Mg}^{2+}$, $M' = \text{Ni}^{2+}$. All compositions in this class, along with unit-cell parameters, are summarized in Table 3. The Co^{2+} and Ni^{2+} compounds show similar colors to the analogous TM phosphites.

Where $M = M'$, the general formula can easily be written in the style of the structure-generating function as



The parameter $x/2$ describes the occupancy of the hexagonal-channel X site. Hydroxyl fully occupies the Φ^H and θ^t sites, and some θ^h sites where X is vacant (Pizarro *et al.* 1993, Marcos *et al.* 1993a, 1995, Hughes *et al.* 2003). Compounds with $x > 1$ necessarily have adjacent non-vacant face-sharing octahedra in the hexagonal channel.

Transition-metal cations, particularly Ni^{2+} , seem to have a significant stereochemical effect on the structure and possible compositions. Marcos *et al.* (1993a) found the composition with minimum x that could be synthesized was ~ 0.76 ; attempts to synthesize compounds with $x = 0$ (*i.e.*, with an empty X site) resulted in a final structure with at least $x = 0.76$. Similarly $x \sim 1.33$ seems to be the maximum for the Ni^{2+} compounds (Marcos *et al.* 1995). At this composition, the X site is $2/3$ occupied, with the hexagonal channel occupied by dimers of face-sharing octahedra ordered such that



with the cations relaxing towards the vacancies. Cation-cation repulsion across the shared face is strong for Ni^{2+} , creating positional disorder at all the heavy-atom sites in the $x = 1.33$ Ni^{2+} arsenate compound (Marcos *et al.* 1995). The authors argued that the strong repulsion between divalent cations is due to the $3d^8$ electronic configuration of Ni^{2+} with its fully occupied t_{2g} orbitals. However, Co^{2+} has both a larger radius (0.74 Å in the electronic high-spin state *versus* 0.69 Å for Ni^{2+}) and the same fully occupied t_{2g} orbitals, yet similar disorder was not reported in the analogous Co^{2+} arsenate (Hughes *et al.* 2003).

In addition to possible stereochemical effects, transition-metal cations in the DLM structure produce characteristic magnetic behavior. All Ni^{2+} , Co^{2+} , and $(\text{Mg}^{2+}, \text{Ni}^{2+})$ compounds follow the Curie-Weiss law above 80 K, with a negative Weiss temperature (Pizarro *et al.* 1993, Rojo *et al.* 2002, Hughes *et al.* 2003).

Antiferromagnetic interactions predominate above 50 K for all the Ni-bearing compounds and the Co^{2+} , As^{5+} compounds (Pizarro *et al.* 1993, Rojo *et al.* 2002, Hughes *et al.* 2003), whereas ferromagnetic interactions predominate in the Co^{2+} , P^{5+} compounds (Pizarro *et al.* 1993). The low temperature (< 50 K) behavior is more complex and depends on occupancy of the X, M, and T sites.

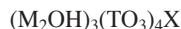
The mixed $(\text{Mg}^{2+}, \text{Ni}^{2+})$ compositions prepared by Rojo *et al.* (2002) have stoichiometries $\text{Mg}_{7.5}\text{Ni}_6\text{H}_3(\text{AsO}_4)_8(\text{OH})_6$ and $\text{Mg}_8\text{Ni}_4\text{H}_6(\text{PO}_4)_8(\text{OH})_6$. Rietveld refinements showed that in the arsenate, M^H is occupied by $\text{Mg}_{0.5}\text{Ni}_{0.5}$ with no order detected, and X is occupied by $\text{Mg}_{0.76}\square_{0.24}$. The phosphate synthesized contained impurities which precluded Rietveld refinement, but the stoichiometry strongly suggests that X is vacant and M^H is occupied by $\text{Mg}_{2/3}\text{Ni}_{1/3}$. Unlike the pure Ni^{2+} phosphates of Pizarro *et al.* (1993) and Marcos *et al.* (1993a), with partial occupancy of Mg^{2+} at the octahedrally coordinated framework sites, H^+ at θ^h in the hexagonal channel is sufficient to charge-balance the framework and tetrahedra, with no X cations needed.

The $\text{T}'\Theta'_3\theta'$ groups in the triangular channel point up with respect to the $\text{T}^h\Theta^h_3\theta^h$ groups in the hexagonal channel in both Co^{2+} (Hughes *et al.* 2003) and Ni^{2+} (Marcos *et al.* 1995) arsenates. Orientations for the $\text{T}'\Theta'_3\theta'$ groups were not determined for the phosphates or for the mixed $(\text{Mg}^{2+}, \text{Ni}^{2+})$ compositions.

Marcos *et al.* (1995) investigated the thermal stability of the Ni^{2+} arsenates and phosphates. They found that upon heating, the pnictogen T^{5+} cations were reduced to T^{3+} as $\text{TO}_3\text{OH}^{2-}$ groups convert to HTO_3^{2-} . The reduction occurs in two stages; in the hexagonal channels from 375 to 500 °C, then in the triangular channels up to 700 °C. A complete collapse of the structure occurs at 830 °C.

TM chalcogenites

The transition metal chalcogenites have the general stoichiometry



with $\text{T} = \text{Se}^{4+}$ or Te^{4+} , $\text{M} = \text{Ni}^{2+}$ or Co^{2+} , and $\text{X} = \text{OH}^-$ or F^- (Perez *et al.* 1976, Marcos *et al.* 1993a, Amorós *et al.* 1996). They are unique among the DLMs in having the X sites in the hexagonal channel occupied by anions.

Both $\text{T}^h\Theta^h_3\theta^h$ and $\text{T}'\Theta'_3\theta'$ are TO_3^{2-} pyramidal groups, with θ^h , θ' representing the stereochemically active lone pairs of electron associated with the T^{4+} chalcogen cation. As in ekatite and the hypothetical Si-free dumortierite-holtite endmembers, this leads to a lack of coordinating anions around the hexagonal channel, and thus no cations at the X site. However, the $[(\text{M}_2\text{OH})_3(\text{TO}_3)_4]^+$ framework is positively charged, and so small monovalent "guest" anions OH^- or F^- are incorporated into the hexagonal channel for charge

balance (Marcos *et al.* 1993a, Amorós *et al.* 1996). The X anions are octahedrally coordinated by the lone pairs of electrons on the chalcogens. The anions Cl⁻ and Br⁻ have ionic radii too large for incorporation into the channel, which has a radius of 1.58 Å as defined by the ring of three T⁴⁺ lone-pairs of electrons (Amorós *et al.* 1996). Infrared spectra of the X = OH⁻ compounds display two OH⁻ stretching bands corresponding to the Φ^H and X sites, whereas X = F⁻ compounds display only one, showing that F in the latter occurs at the X sites exclusively rather than being distributed over both sites (Amorós *et al.* 1996).

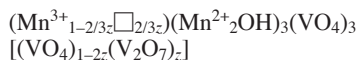
In the triangular channel, the T'ⁱΘ'₃θ' groups point down with respect to the T^hΘ^h₃θ^h groups for M = Ni²⁺, Co²⁺ and T = Se⁴⁺, Te⁴⁺, contrary to most other DLMs except the Ni²⁺ phosphite. The Ni²⁺ and Co²⁺ chalcogenites show the same coloration as the corresponding Ni²⁺ and Co²⁺ phosphites, phosphates and arsenates.

Metal vanadates and sulfate-vanadates

Open-framework vanadium oxides are of interest to solid-state chemists owing to their potential use as secondary cathode materials in advanced lithium batteries (Zhang *et al.* 1999, Hu *et al.* 2008). Vanadate DLMs have been investigated during this research, along with the similar lyonsite-like compounds discussed below.

Kato *et al.* (1998) synthesized the compound Zn(Zn₂OH)₃(VO₄)₃(SO₄) with Zn²⁺ at the X and M^H sites, VO₄³⁻ as the T^hΘ^h₃θ^h groups lining the hexagonal channel, and SO₄²⁻ as the T'ⁱΘ'₃θ' groups in the triangular channel (pointing up with respect to the T^hΘ^h₃θ^h groups). One hydrogen is attached to the Φ^H oxygen atom. Although Zn occupancy of the X site was not refined, it is unlikely to be fully occupied, on the basis of other DLMs described. In this case, additional H⁺ should be present as well, most likely as VO₃OH²⁻ (with OH⁻ at the θ^h position pointing into the hexagonal channel) but also possibly as SO₃OH⁻ in the triangular channel. Whereas Kato *et al.* (1998) did not address mixing of S⁶⁺ and V⁵⁺ between the two tetrahedrally coordinated sites, bond lengths are consistent with a complete order of V⁵⁺ at T^h and S⁶⁺ at T'.

Two vanadate-only DLM compositions have been synthesized, with Mn and Mg as the octahedrally coordinated metal cations. Zhang *et al.* (1999) synthesized the Mn vanadate

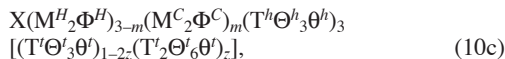


with $z = 0.199$. The triangular channel contains both upward-pointing VO₄³⁻ tetrahedra and apex-sharing V₂O₇⁴⁻ pairs of tetrahedra. Two distinct V sites in the triangular channel, one above the ring of three basal Θ' oxygen atoms and one below, indicate that like the Co²⁺ phosphite mentioned above, the triangular channel

contains both upward- and downward-pointing VO₄³⁻ tetrahedra (with z the fraction of downward-pointing groups). However, unlike the Co²⁺ phosphite, there are not two distinct θ' oxygen sites, meaning that adjacent T'ⁱΘ'₃θ' groups of opposite orientations must either be separated by vacancies (Fig. 6C) or share apical oxygen atoms (Fig. 6D); face-sharing tetrahedra place the V⁵⁺ cations far too close to each other and so are ruled out. In the former case, the triangular channel contains randomly oriented single VO₄³⁻ tetrahedra, and there is exactly one apical θ' oxygen atom per occupied tetrahedron. In the second case (Fig. 6D), the triangular channel contains both single upward-pointing VO₄³⁻ tetrahedra and pairs of tetrahedra that share an apical θ' oxygen atom,



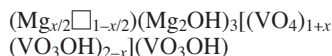
In this case, there are only as many θ' oxygen atoms as there are upward-pointing tetrahedra, so the occupancy of θ' equals the occupancy of the upward-pointing T' site. Zhang *et al.* (1999) found significant θ' vacancies, approximately equal to the population of down-pointing tetrahedra in the triangular channel, and so concluded that the triangular channel of the Mn vanadate resembles that shown in Figure 6D (See also Ch. 23 in Pecharsky & Zavalij 2009). The structure-generating function can be modified to include apex-sharing T'ⁱΘ'₃θ' groups as



where $0 \leq z \leq 1/2$ indicates the degree of polymerization in the triangular channel.

For charge balance, Mn in the hexagonal channel X site is assigned a valence of 3+. The material decomposes into Mn²⁺₂V₂O₇ and Mn³⁺₂O₃ between 400 and 550 °C in oxygen (Zhang *et al.* 1999), which suggests that both valence states of Mn may be present at room temperature. No H positions other than Φ^H were found, although bond-valence analysis of the published structure suggests that θ' is likely occupied by OH⁻ whereas θ^h in the hexagonal channel is dominated by O²⁻.

Hu *et al.* (2008) and Đođević *et al.* (2008) synthesized the similar compound

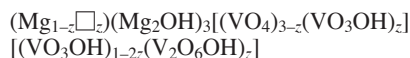


with $x = 0.30$. In this case, charge balance for vacancies in the hexagonal channel are provided by OH⁻ at the θ^h and θ' sites, similar to the metal pnictates. Bond-valence analysis of the published structures suggests that Φ^H and θ' are fully occupied by OH⁻ and θ^h is occupied by both O²⁻ and OH⁻. Infrared spectra (Đođević *et al.* 2008) show the presence of strong hydrogen bonds between θ' and Φ^H and weak hydrogen bonds between Φ^H and θ'.

As with the Mn vanadate, both upward- and downward-pointing $T^i\theta^j\theta^k$ groups are present in the triangular channel with a single θ^l site: 35% and 29% point down in Hu *et al.* (2008) and Đodević *et al.* (2008), respectively. In neither case was the θ^l occupancy refined, so it is undetermined whether the triangular channel contains isolated upward- and downward-pointing VO_4^{3-} tetrahedra or $V_2O_7^{4-}$ pairs. (Hu *et al.* 2008, likewise did not refine the X site occupancy.) If the structure is the same as the Mn vanadate and contains upward-pointing VO_4^{3-} groups and $V_2O_7^{4-}$ pairs, the stoichiometry is modified to



Đodević *et al.* (2008) found an X site occupancy ($x/2 = 0.698$) approximately equal to the independently refined occupancy of up-oriented T sites ($1 - z = 0.706$); if this is generally true, then the simplified stoichiometry is



The V–O bond length in the VO_4^{3-} tetrahedra varies considerably among the three vanadate materials. Among the T^h groups, the V–O bond lengths range from 1.694 to 1.729 Å in the Zn sulfate-vanadate (Kato *et al.* 1998), from 1.629 to 1.700 Å in the Mn vanadate (Zhang *et al.* 1999), and from 1.699 to 1.736 Å (Hu *et al.* 2008) and 1.704 to 1.734 Å (Đodević *et al.* 2008) in the Mg vanadate. Among the triangular channel groups, the bond lengths range from 1.664 to 1.963 Å in the Mn vanadate (Zhang *et al.* 1999) and 1.701 to 1.905 Å (Hu *et al.* 2008), and 1.711 to 1.93 Å (Đodević *et al.* 2008) in the Mg vanadate. The exceptionally long bonds are all $T^i\theta^j$ bonds.

Crystals of the Mn vanadate are dark brown in color, while the Mg vanadate ranges from yellow (Hu *et al.* 2008) to light orange (Đodević *et al.* 2008), all typical colors for V^{5+} compounds. Crystals of the Zn sulfate-vanadate range from colorless to pale purple.

Unit-cell parameters: *a/c*

Using a simple model based on the underlying {6·4·3·4} net and undistorted coordination octahedra, we calculated above that in both orthorhombic and hexagonal DLMs, the ratio of *a* and *c* unit-cell parameters should be close to

$$\frac{a}{c} = \frac{3}{2} + \frac{2\sqrt{2}}{3} \approx 2.443 \quad (6)$$

i.e., approximately four times that of a hexagonally close-packed unit cell.

The *a* and *c* unit-cell parameters of 102 natural and synthetic DLMs, both orthorhombic and hexagonal, are plotted in Figure 8; these include data for dumortierite-group minerals from the same sources as Figure 5 as well as data for ellenbergerite (5 natural samples), phosphoellenbergite (1 natural and 4 synthetic samples), ekatite (1 natural sample), and synthetic DLMs (30 samples of diverse chemistry). All show *a/c* ratios significantly higher than the approximation of equation 6, from 2.47 (for the carbonate-bearing phosphoellenbergerite from Modum: Raade *et al.* 1998) to 2.62 (for the Ni tellurite with OH at the X site: Perez *et al.* 1976). Averages and ranges for different groups of DLMs are given in Table 4.

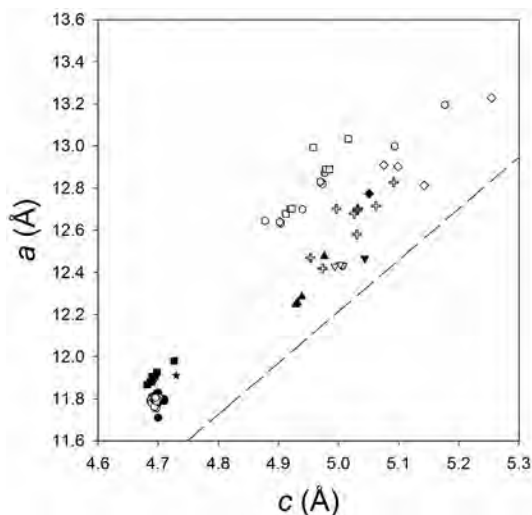


FIG. 8. Unit-cell parameters *a* versus *c* for DLMs. Sources for naturally occurring dumortierite (black circles), synthetic dumortierite (white circles), holtite (black squares), and magnesioldumortierite (black star) are given in the caption to Fig. 5. Black triangles represent ellenbergerite [2 data from Comodi & Zanazzi (1993a), one each from Chopin *et al.* (1986), Comodi & Zanazzi (1993b), and Zubkova *et al.* (2007)]; black inverted triangles, natural phosphoellenbergerite [from Raade *et al.* (1998)]; white inverted triangles, synthetic phosphoellenbergerite [4 data from Brunet *et al.* (1998)]; black diamonds, ekatite [from Keller (2001)]; white hexagons, TM phosphites [2 data from Marcos *et al.* (1993b), 2 from Atfield *et al.* (1994), 2 from Ni *et al.* (2009), and one each from Marcos *et al.* (1993c), Che *et al.* (2005), Gu *et al.* (2007), and Liao & Ni (2010)]; white crosses, metal pnicates [3 data from Marcos *et al.* (1993a), 2 from Marcos *et al.* (1995), 2 from Hughes *et al.* (2003), and 2 from Rojo *et al.* (2002)]; white squares, TM chalcogenites [4 data from Amorós *et al.* (1996), 2 from Perez *et al.* (1976), and one from Marcos *et al.* (1993a)]; white diamonds, metal vanadates and sulfate-vanadates [one each from Kato *et al.* (1998), Zhang *et al.* (1999), Đodević *et al.* (2008), and Hu *et al.* (2008)]; the dashed line is the calculated *b/a* ratio (equation 6). Error bars on each point are smaller than the symbols.

There is a significant gap between the orthorhombic dumortierite-group minerals, clustered tightly together in the lower left corner of the plot, and the hexagonal materials. The dumortierite-group minerals have smaller unit-cell parameters than the hexagonal DLMs, largely because Al^{3+} is significantly smaller than the divalent cations that dominate the hexagonal DLMs; $V_{\text{r,Al}} = 0.54 \text{ \AA}$ versus 0.69 \AA for Ni^{2+} , 0.72 \AA for Mg^{2+} , 0.74 \AA for Co^{2+} and Zn^{2+} , and 0.78 \AA for Fe^{2+} (Shannon 1976), and as Figure 7 shows for synthetic TM phosphites, the unit-cell parameters depend strongly on the size of the M cation. The hexagonal DLMs are spread over a wider region of the plot than the orthorhombic dumortierite group, most likely owing to the greater variation in composition at both octahedrally and tetrahedrally coordinated sites.

In general we find that the a and (in orthorhombic minerals) b unit-cell parameters vary with the size of the T^h groups, whereas c is largely independent or only weakly dependent on T^h size; thus the Co and Ni tellurites have the highest a parameters and a/c ratios, as TeO_3^{2-} has Te–O bond lengths around 1.88 \AA (Shannon 1976). This effect was investigated by Marcos *et al.* (1993a). Figure 9A shows a versus average tetrahedral bond length in Co and Ni DLMs with $\text{T}^h = \text{T}^t$ (with data from Perez *et al.* 1976, Marcos *et al.* 1993a,b,c, Amoros *et al.* 1996, and Hughes *et al.* 2003). For both Co and Ni compounds, there is a roughly uniform increase of a as T–O bond length increases across the phosphates, arsenates, selenites, and tellurites. No clear dependence is apparent in the c unit-cell parameter (Fig. 9B).

If the Co and Ni phosphites are added to the same graphs, either versus the average of all four P–(O,H)

bonds (triangles in Figs. 9A,B) or the average of the three P–O bonds only (squares), we see that the a parameter is significantly greater (by at least 0.3 \AA for Co, 0.2 \AA for Ni) than expected from the other materials. The HPO_3^{2-} groups seem to be behaving like much larger tetrahedra than they actually are. The cause of this anomaly is not clear. In the phosphites, the P–H bonds extend into the hexagonal channel, and the X sites are empty owing to a lack of coordinating oxygen atoms. The vacancies at the X site alone are not enough to be responsible for the expansion of a , because the a parameters of the selenites and tellurites, which also have empty channels, are not anomalously large in comparison to the phosphates and arsenates; in particular, the mean $\text{Se}^{4+}\text{--O}$ and $\text{As}^{5+}\text{--O}$ bond lengths are similar ($\sim 1.7 \text{ \AA}$), and these materials have similar a parameters ($\sim 12.7 \text{ \AA}$), although the arsenates have occupied X sites. Similarly, the stoichiometry of the mixed Mg–Ni phosphate (Rojó *et al.* 2002) suggests that it too has an empty hexagonal channel (and similar cation radii for Mg^{2+} and Ni^{2+} , 0.72 \AA and 0.69 \AA respectively), and it has a similar a (12.42 \AA) to the Ni^{2+} phosphate of Marcos *et al.* (1993a) (12.47 \AA), which has a 34% occupied X site. The remaining major difference between the phosphates and the phosphites is the dangling H ions in the hexagonal channel in the latter; electrostatic repulsion may be sufficient to cause an expansion in the plane normal to the c -axis to increase the distance between adjacent H atoms.

There is a similar dependence on the mean size of T^h groups in the orthorhombic minerals; in the dumortierite-holtite solid-solution a and b increase with increasing AsO_3^{3-} and SbO_3^{3-} content (which leads to

TABLE 4. UNIT-CELL RATIOS FOUND IN DLMs. AVERAGES (WITH STANDARD DEVIATION) ARE GIVEN FOR MINERALS, RANGES FOR SYNTHETIC MATERIALS, WHEN $N > 1$.

	N	a/c	b/a
Dumortierite	30	2.512(5)	1.714(5)
Dumortierite (synthetic)	21	2.503 - 2.516	1.712 - 1.726
Holtite	9	2.536(2)	1.713(2)
Magnesioldumortierite	1	2.518	1.713
Ellenbergerite (ordered, space group $P6_3$)	4	2.486(1)	
Ellenbergerite (disordered, space group $P6_3ma$)	1	2.507	
Phosphoellenbergerite	1	2.472	
Phosphoellenbergerite (synthetic)	4	2.482 - 2.489	
Ekatite	1	2.529	
TM Phosphites	10	2.549 - 2.592	
Metal Pnictates (Phosphates, Arsenates)	9	2.497 - 2.542	
TM Chalcogenites (Selenites, Tellurites)	7	2.581 - 2.621	
Zn Sulfate–Vanadate	1	2.492	
Metal Vanadates	3	2.518 - 2.544	
	102	2.52(3)	

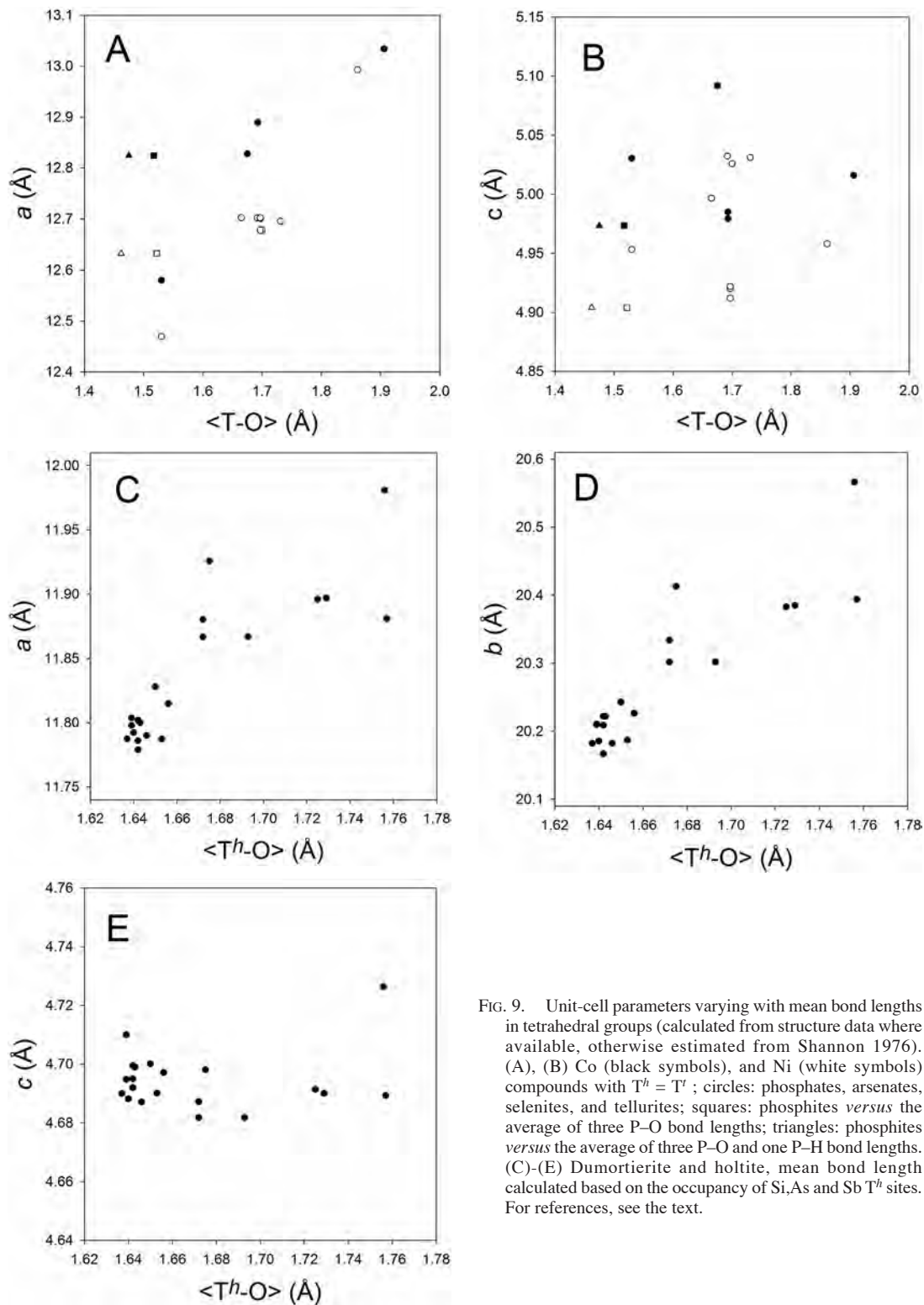


Fig. 9. Unit-cell parameters varying with mean bond lengths in tetrahedral groups (calculated from structure data where available, otherwise estimated from Shannon 1976). (A), (B) Co (black symbols), and Ni (white symbols) compounds with $T^h = T^l$; circles: phosphates, arsenates, selenites, and tellurites; squares: phosphites *versus* the average of three P-O bond lengths; triangles: phosphites *versus* the average of three P-O and one P-H bond lengths. (C)-(E) Dumortierite and holtite, mean bond length calculated based on the occupancy of Si,As and Sb T^h sites. For references, see the text.

increasing average T^h -O) whereas c remains essentially flat at comparable scales (Figs. 9C-E, with data from Moore & Araki 1978b, Alexander *et al.* 1986, Hoskins *et al.* 1989, Fuchs *et al.* 2005, Zubkova *et al.* 2006, Kazantsev *et al.* 2006, Groat *et al.* 2009, 2012, Evans *et al.* 2012, and one unpublished data set on holtite). Substitutions at the octahedrally coordinated sites introduce additional scatter but an increasing trend is clear.

Summary

We have seen that the dumortierite-like materials are a group of natural and synthetic materials with highly diverse chemical compositions, and structures that can be described by the generalized structure-generating function (expression 10a) $X(M_2\Phi)_3(T^h\Theta^h_3\theta^h)_3(T^i\Theta^i_3\theta^i)$. The structure-generating function encapsulates a structure based on the {6·4·3·4} semi-regular tiling, with wide hexagonal and smaller triangular channels, created by a framework of double-chains of octahedra. The double-chains are of two types: chains of face-sharing dimers of octahedra, resulting in a hexagonal close-packed rod (M^H chain), and chains of staggered edge-sharing octahedra which form a cubic close-packed rod (M^C chain); the hexagonal structure contains only M^H chains whereas the orthorhombic structure contains M^C and M^H chains in a 2:1 ratio. The triangular channels contain tetrahedral, trigonal pyramidal or trigonal planar $T^i\Theta^i_3\theta^i$ groups. The hexagonal channels are lined by tetrahedral or trigonal pyramidal $T^h\Theta^h_3\theta^h$ groups. Where present, the apical θ^h anions create a chain of face-sharing X octahedra, which are generally only partly occupied, parallel to the c -axis down the center of the hexagonal channel.

Occupancy of the X sites is controlled in part by the need to charge-balance the combination of the double-chain M framework and the T^h and T^i groups, that is, the 'decorated framework' $[(M_2\Phi)_3(T^h\Theta^h_3\theta^h)_3(T^i\Theta^i_3\theta^i)]^{q-}$. In the majority of DLMs, the decorated framework has a net negative charge, and so cations are distributed over the X sites for charge balance, *i.e.*, $X = (M^i, \square)^{q+}$. Additional constraints on this distribution are imposed by the nature of the coordinating θ^h , as O^{2-} and OH^- will coordinate a cation at the X site, but H^- or a lone pair of electrons will not, and by repulsion between the cations: for example, the distance between X sites in holtite is too short for adjacent sites to be occupied by Ta^{5+} , so these cations must be separated by a vacancy. In some DLMs, the decorated framework has a net positive charge. In the phosphites, this is charge-balanced by an empty X site and a partial vacancy at the M^H site, bringing the net charge on the decorated framework to zero. In the chalcogenites, this is charge-balanced by filling the X sites with OH^- and F^- .

The structure and symmetry of the DLMs lead to certain common properties. The unit-cell parameters and ratios between them can be estimated reasonably well on the basis of the geometry of the {6·4·3·4} tiling

and idealized chains of octahedra. The framework of rod-like components (the double-chains of octahedra) leads to crystals that are needle- or fiber-like, and generally hexagonal or pseudohexagonal at the microscopic scale. Micrographs of synthetic crystallites (*e.g.*, Marcos *et al.* 1993b, Zhang *et al.* 1999, Gu *et al.* 2007, Ni *et al.* 2009, Liao & Ni 2010) strikingly resemble the crystal forms of dumortierite (see in particular Fig. 8 of Schaller 1905). In the dumortierite-group minerals, the strongly pseudohexagonal structure leads to commonly-observed twinning along axes parallel to the structure's near-threefold symmetry axes.

Examining the commonalities among DLMs can be helpful in deciding questions about the crystal chemistry of dumortierite. For example, the synthetic DLMs incorporate OH^- at the four-coordinate Φ^H sites and the apical θ^h and θ^i sites. In the dumortierite-group minerals, the O2 and O7 (θ^h) sites are generally believed to host OH^- , but whether the O10 (Φ^H) site hosts OH^- , as suggested by bond-valence calculations, is less certain. The dominance of OH^- at Φ^H sites in synthetic DLMs and in ellenbergerite-group minerals strongly suggests that O10 in the dumortierite-group minerals should contain significant OH^- . Bond-valence sums for O10 in dumortierite-group minerals are typically 1.5-1.7 valence units (*vu*), *versus* an ideal 2.0 *vu* for O^{2-} and 1.0 for OH^- , so that OH^- occupation is only partial.

As explained by Alexander *et al.* (1986), the affinity of Φ^H sites for OH^- comes from local distortions of the M^H double-chain. In the M^H -type double-chains, the four-coordinate vertices are in a flattened square-pyramidal arrangement. Assuming undistorted M^H octahedra with M^H -O bonds of 1.90 Å, the square pyramid has an apical angle of 132° and the apex (Φ^H) is 0.78 Å from the center of the base. But with these ideal octahedra, the shortest edge of the pyramid (that is, the shortest M^H - M^H distance) is only 2.19 Å. The real M^H polyhedron is considerably distorted to prevent this; as Alexander *et al.* (1986) describe it, contraction of the five shared edges leads to a very asymmetrically distorted octahedron. The minimum Al-Al distance between Al4 sites increases to 2.56 Å (structural data from Evans *et al.* 2012), but the Φ^H pyramid is even flatter, with apical angle 151° and the apex only 0.50 Å from the center of the base. This also results in one very long M^H - Φ^H bond in the M^H octahedron (2.016 Å *versus* the average 1.895 Å for Al4-O in dumortierite; other DLMs show similarly long bonds), which is primarily responsible for the low incident bond-valence of the Φ^H anion, making it a desirable site for OH^- .

The Al4 octahedron is the most distorted of the four octahedrally coordinated sites in dumortierite, with a quadratic elongation (QE) of 1.0187 and a bond angle variance (BAV) of 0.0185 radians², compared with Al1 (QE 1.0042, BAV 0.0046) and Al2, Al3 (QE 1.0141, BAV 0.0142). Similar degrees of distortion occur in other DLMs.

What about the other four-coordinate oxygen site in the dumortierite structure, the Φ^C position in the M^C -type double-chains? Despite the local bond-topological similarities between the M^H - and M^C -type chains, and the identical roles they play as structural elements, geometrically the two local environments are quite different. The M^C octahedra have only four shared edges each, and although these are again contracted the overall polyhedral distortion is less. The local coordination geometry of the Φ^C site is that of a distorted tetrahedron (actually close to an octahedron with two *cis* vertices deleted), with a minimum M^C - M^C distance of 2.85 Å. The Φ^C oxygen atom is thus fully satisfied and an extra H atom is not needed.

The dumortierite-group minerals contain the trigonal planar BO_3^{3-} group in their triangular channels, but both the ellenbergerite-group minerals and synthetic DLMs feature tetrahedral or trigonal pyramidal $T'\Theta'_3\theta'$ groups. In ekatite and the TM chalcogenites, the atom at θ' has a lone pair of electrons, and the group is a trigonal pyramid. In the remaining DLMs, θ' is an anion (O^{2-} or OH^- or H^-) and the group is tetrahedral. The only other trigonal planar group found in DLMs is CO_3^{2-} in phosphoellenbergerite (Raade *et al.* 1998), which does not dominate the triangular channel. In hexagonal DLMs, the uniform orientation of the $T^h\Theta^h{}_3\theta^h$ groups defines a unique "up" direction along the *c*-axis (Fig. 6A), and so in the triangular channel, non-planar $T'\Theta'$ groups may point up, down, or both. Most hexagonal DLMs have $T'\Theta'_3\theta'$ groups pointing up: ellenbergerite, phosphoellenbergerite and ekatite, and the Zn, Fe, and Mn phosphites, Ni and Co arsenates, and the Zn sulfate-vanadate. However, the Ni phosphite and all TM chalcogenites (Ni and Co selenites and tellurites) have $T'\Theta'$ groups pointing down, and others are mixed: Co phosphite (80% down), Mn vanadate (80% up), and Mg vanadate (65-70% up). In the Mn and Mg vanadates, adjacent upward- and downward-pointing $T'\Theta'$ groups share apices forming $T'_2\Theta'_6\theta'$ groups; this does not seem to occur in the Co phosphite, as upward- and downward-pointing $T'\Theta'_3\theta'$ groups have distinct θ' sites.

What determines the orientation of tetrahedral or pyramidal groups in the triangular channel? Is there a crystal-chemical reason why certain compositions favor one orientation over the other or a disordered mix of orientations, or could this be a function of synthesis conditions? These questions should be investigated in any future program of syntheses and structure refinement of DLMs.

In the orthorhombic DLM structure, the $T^h\Theta^h{}_3\theta^h$ groups may define a local up direction in individual hexagonal channels but not globally for the structure, as $T^h\Theta^h{}_3\theta^h$ groups point in opposite directions in alternating rows of hexagonal channels (see Fig. 4B, slabs of type 1 *versus* type $\bar{1}$). The $T'\Theta'_3\theta'$ groups in the triangular channels would likely alternate in a similar way. The dumortierite-group minerals avoid

this issue by incorporating only planar BO_3^{3-} groups. No substitution for boron has yet been reported in any dumortierite-group mineral.

CLOSELY RELATED STRUCTURES

Next, we discuss structures that are closely related to the dumortierite structure: the lyonsite structure, which replaces the double-chains of octahedra in dumortierite with single chains of octahedra and trigonal prisms; the satterlyite-holtedahlite structure, which is built of trimers of M^H -type double-chains of octahedra assembled in a different way; and the cancrinite AB-polytype, which is based on the same cation lattice as the hexagonal DLM structure.

The lyonsite structure

Lyonsite, $\alpha\text{-Cu}_3\text{Fe}_4(\text{VO}_4)_6$, has the crystal structure (space group *Pmcn*) shown in Figure 10A, which we shall refer to as the lyonsite structure. It is strikingly similar to the dumortierite structure, with a chain of face-sharing octahedra connected via pinwheels of tetrahedral groups to a framework of chains of 6-coordinate metals in an orthorhombic variation of the {6·4·3·4} semi-regular tiling. The key difference is that in lyonsite there are single chains of edge-sharing octahedra and trigonal prisms in a 2:1 ratio, instead of double-chains of octahedra (Fig. 10B). This shrinks the triangular channels so that there is no longer room for $T'\Theta'_3\theta'$ groups.

In addition to lyonsite (Hughes *et al.* 1987), many synthetic compounds with the same structure incorporate diverse 6-coordinate cations with valencies from 1+ to 5+, although with the exception of Na^+ and Cu^+ , all with cation radii between 0.65 and 0.75 Å. The tetrahedrally coordinated cations are thus far restricted to V^{5+} , Mo^{6+} , W^{6+} , or a disordered mix of two of these, with the majority of compositions lithium molybdates. A thorough review is given by Smit *et al.* (2006a). By analogy with the DLMs, we refer to any mineral or synthetic compound with the lyonsite structure as a lyonsite-like material (LLM).

The corresponding changes to the generalized structure-generating function (expression 10a) for the lyonsite structure are straightforward; the general double-chain term $M_2\Phi$ is replaced by M for a single chain and the $T'\Theta'_3\theta'$ term is dropped, giving



for the generalized lyonsite structure-generating function. Note that all anions in the structure are now at most 3-coordinate. Representing the octahedrally coordinated single chain sites by M^O and the trigonal-prism sites by M^P , a full structure-generating function for lyonsite can be written



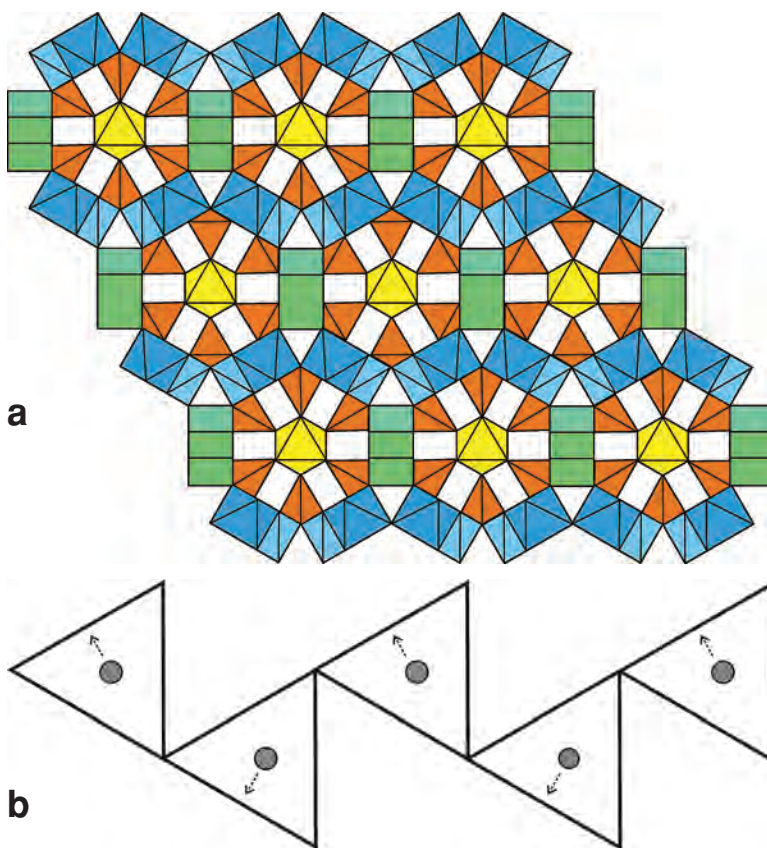


FIG. 10. (A) The lyonsite structure viewed down the c -axis. Face-sharing X octahedra are shown in yellow, T^h tetrahedra in orange, M^O single chain octahedra in blue, and M^P triangular prisms in green. (B) Edge-sharing chain of M^P triangular prisms. Arrows show displacement of cations from the prism's center in distorted coordination environments.

More rigorously, in the lyonsite structure, the coordination of the M site becomes $M(\Theta^{h_{1/3}})_6 = M\Theta^{h_2}$, and with now two M per {4} instead of four, equation (9a) becomes $\{4\} = [M\Theta^{h_2}]_2$. Equation (9b) for the {6} channel is unchanged, and with the {3} channels empty, equation (9c) becomes simply $\{3\} = []$. The {6-4-3-4} tile stoichiometry then gives

$$\begin{aligned} \{6\}\{4\}_3\{3\}_2 &= [XT^h_3\Theta^h_3\theta^h_3]_2[M\Theta^h_2]_6[l]_2 \\ &= 2[XM_3(T^h\Theta^h_3\theta^h_3)] \end{aligned}$$

Comparing expressions 10a and 11a, we can further generalize a structure-generating function for structures based on frameworks of n -tuple 6-coordinate chains in a {6-4-3-4} net:

$$X_2(M_n\Phi_{n-1})_6(T^h\Theta^h_3\theta^h_3)_6[(T^h\theta^h)_n\Theta^h_{n+4}]_{n-1} \quad (12)$$

where $n = 1$ corresponds to lyonsite and $n = 2$ to the dumortierite- and ellenbergerite-group minerals. The size of the triangular channel increases with n . A hexagonal version of the hypothetical $n = 3$ structure is shown in the deposited Supplementary Figure S2 (available from the Mineralogical Association of Canada Depository of Unpublished Data, document Dumortierite CM50_1197).

The first LLM was discovered by Smith (1960) during an investigation of desulfurization catalysts used in petroleum refinement, a mixture of alumina laced with Co and Mo oxides (it was these oxides Smith was attempting to characterize). Single crystals in the form of deep blue needles and platelets were synthesized in a melt of sodium molybdate and anhydrous cobalt chloride with NaCl as a flux. The space group and unit-cell parameters (equivalent to $Pm\bar{c}n$,

$a = 10.778$, $b = 18.017$, and $c = 5.245$ Å; as with the dumortierite-group minerals, both *Pnma* ($a < b < c$) and *Pmcn* ($c < a < b$) settings are used for LLMs with such symmetry) were determined from Weissenberg photographs, and the Co and Mo positions were determined using Patterson methods. From this partial structure solution, the underlying pseudo-hexagonal net {6·4·3·4} was visible. The full structure of the material determined to be $\text{NaCo}_{2.31}(\text{MoO}_4)_3$ was described by Ibers & Smith (1964). Later, Klevtsova & Magarill (1970) synthesized the first Li molybdates, $\text{Li}_2\text{Fe}_2(\text{MoO}_4)_3$ and $\text{Li}_3\text{Fe}(\text{MoO}_4)_3$, and identified their structures as that described by Ibers & Smith (1964). Other LLMs were rapidly produced as the materials hold interest as potential catalysts for selective oxidation of hydrocarbons (Smit *et al.* 2006a) and as ionic conductors (Sebastian *et al.* 2003).

Lyonsite, $\alpha\text{-Cu}_3\text{Fe}_4(\text{VO}_4)_6$, was found in summit crater fumaroles of the Izalco volcano, El Salvador, among minerals formed as sublimate products from volcanic gases (Hughes *et al.* 1987). It has space group *Pmcn*, $a = 10.296$, $b = 17.207$, and $c = 4.910$ Å, and empirical composition $\text{Cu}_{1.52}\text{Fe}^{3+}_{1.73}\text{Mn}^{3+}_{0.24}\text{Ti}^{4+}_{0.16}(\text{V}_{0.97}\text{O}_4)_3$. Copper appears to be predominantly divalent, although some monovalent Cu may be present as well. The connection with the growing family of synthetic compounds was not immediately made, although Hughes *et al.* (1987) did recognize the kinship with dumortierite. The connection between lyonsite and the Ibers & Smith (1964) structure was made by Wang *et al.* (1996).

Although LLMs possess three distinct types of 6-coordinate sites, most do not show a clear order of cations. Low-valence cations (Li^+ and Na^+) seem to prefer the prismatic M^P sites (Smit *et al.* 2006a). High-valence cations (*i.e.*, 4+ or 5+) may prefer X sites (Klevtsova *et al.* 1979, Smit *et al.* 2006a, 2008) buffered by vacancies or low-valence cations. Compositions where the average valence at M^O is greater than the average valence at X (*e.g.*, Ozima *et al.* 1977, Hughes *et al.* 1987, Wang *et al.* 2000), and the converse (Klevtsova *et al.* 1979, Sebastian *et al.* 2003) have both been observed.

As in DLMs, the X sites may have a high vacancy content, with up to 50% reported (Klevtsova *et al.* 1979). Conversely, compositions in the series $\text{A}^2\text{M}^{2+}_2(\text{MoO}_4)_3$ and $\text{A}^3\text{M}^{3+}(\text{MoO}_4)_3$, with A^+ mostly Li^+ or occasionally Na^+ , have been found to be vacancy-free, likely because X sites occupied by A^+ are nearly as good as vacancies for separating more highly charged cations. Smit *et al.* (2006b) found complete solid-solution between the vacancy-free $\text{Li}_2\text{Mg}_2(\text{MoO}_4)_3$ and $(\text{Mg}_{0.75}\square_{0.25})\text{Mg}_3(\text{V}_{0.5}\text{Mo}_{0.5}\text{O}_4)_3$. Those LLMs with substantial vacancies (like DLMs) have high anisotropies at the X sites (*e.g.*, Katz *et al.* 1971, Hughes *et al.* 1987, Wang *et al.* 1996, 2000, Smit *et al.* 2008), suggesting relaxation of cations toward adjacent vacancies. In the aforementioned Mg vanadomolybdate, Smit

et al. (2006b) suggested trimers of face-sharing Mg^{2+} octahedra in the hexagonal channel with relaxed end positions, similar to those observed in dumortierite by Evans *et al.* (2012). The X sites in vacancy-free compositions tend to have anisotropies similar to the M^O sites (*e.g.*, Klevtsova & Magarill 1970, Sebastian *et al.* 2003).

In the high-valence compositions $\text{Li}_{3.35}\text{Ta}^{5+}_{0.53}(\text{MoO}_4)_3$ (Smit *et al.* 2006a) and $\text{Li}_2\text{Zr}^{4+}(\text{MoO}_4)_3$ (Klevtsova *et al.* 1979), order of the high-valence cation and (Li^+ , \square) at the X site doubles the c-axis and reduces a mirror plane to a 2_1 screw axis, converting the space group to *Pmn*2₁. Such order is conceivable in dumortierite-group minerals but has not yet been observed.

Several LLMs have been synthesized with both VO_4^{3-} and MoO_4^{2-} or WO_4^{2-} as the $\text{T}^h\Theta^h_3\theta^h$ groups (Wang *et al.* 1996, Pless *et al.* 2006). None show long-range order of V^{5+} and $\text{Mo}^{6+}, \text{W}^{6+}$ at the T^h sites; however, Raman spectroscopy (Pless *et al.* 2006, Smit *et al.* 2006b), EXAFS and computational modeling (Smit *et al.* 2007) suggest that local order places Mo^{6+} or W^{6+} near X vacancies over V^{5+} .

The chains of edge-sharing trigonal prisms are an unusual feature of the lyonsite structure. Sebastian *et al.* (2003) showed that the series $\text{Li}_{2-x}\text{Mg}_{2+x}(\text{MoO}_4)_3$ and $\text{Li}_3\text{M}^{3+}(\text{MoO}_4)_3$ show good ionic conductivity that increases with Li content, with conduction occurring parallel to the c-axis along the M^P chains. This suggests that some vacancies assigned to the X sites may actually occur at the M^P sites.

Some Cu and Zn LLMs, including lyonsite itself, show significant distortion from regularity around the M^P sites. The M^P cation is generally coordinated to four OA and two OB oxygen atoms (labeled O7 and O2, respectively, in Hughes *et al.* 1987), and the prism is defined by the three parallel edges OA–OA, OA–OA, and OB–OB. The two OA–OA edges are shared with adjacent prisms in the chain, whereas the OB vertices are shared with individual M^O octahedra. As is typical for coordination polyhedra, the shared edges are shorter than the unshared edge. The six bond lengths are approximately uniform, with the M^P –OB bond lengths intermediate between two M^P –OA distances; *e.g.*, from Klevtsova & Magarill (1970), M^P –OB = 2.176 Å and M^P –OA = 2.164, 2.186 Å for $\text{Li}_2\text{Fe}_2(\text{MoO}_4)_3$ ($M^P = \text{Li}^+$). This is the situation for most LLMs. However, in several LLMs with Cu or Zn at the M^P sites, the cation is pushed towards one of the square faces of the prism, as indicated by the arrows in Figure 10B, significantly increasing one set of M^P –OA distances. In lyonsite, this distortion transforms the trigonal prism into a site with square planar coordination with M^P –OA_{short} = 1.982 Å, M^P –OB = 1.963 Å, M^P –OA_{long} = 2.575 Å (Hughes *et al.* 1987). In other compositions, the Cu or Zn cation moves toward one OB vertex, creating one very long M^P –OB distance (~2.7 Å) and transforming the prism into a distorted square pyramid. In this case, the distortion is severe enough to reduce

the glide plane parallel to the c -axis to a 2_1 screw axis, reducing the space group of the entire structure from $Pm\bar{c}n$ to $P2_12_12_1$ (Wang *et al.* 1997). This occurs for $(\text{Cu}_{0.85}\square_{0.15})\text{Cu}_3(\text{MoO}_4)_3$ (Katz *et al.* 1971); $(\text{Cu}, \text{Zn})_{3.75}(\text{MoO}_4)_3$ (Szillat & Müller-Buschbaum 1995); $(\text{Cu}, \text{Fe})_{3.63}(\text{MoO}_4)_3$ (Sedello & Müller-Buschbaum 1996); and $(\text{Zn}_{0.77}\square_{0.23})\text{Zn}_3(\text{VO}_4)_{1.54}(\text{MoO}_4)_{1.46}$ (Wang *et al.* 1997). These distortions are attributed to the Jahn-Teller effect for Cu^{2+} , but the origin of the distortion in the Zn compound is unclear (Wang *et al.* 1997).

No hexagonal analogue of the lyonsite structure, containing only chains of M^O octahedra (or only chains of M^P trigonal prisms), analogous to the hexagonal variant of the dumortierite structure, has been reported so far. Such a structure is not ruled out by component-matching rules like an M^C -only dumortierite structure.

Estimates of unit-cell parameter ratios in the lyonsite structure can be calculated by the same method as for the dumortierite structure, on the basis of model octahedra and the underlying $\{6\cdot4\cdot3\cdot4\}$ tiling (Figs. 2 and 1B, respectively). As before, equation 1 gives $a = \sqrt{3}s + s'$, $b = 3s + \sqrt{3}s'$ and $b/a = \sqrt{3} \approx 1.732$, as expected from the symmetry of the tiling. Assuming ideal octahedra with bond length d and height $h = (2\sqrt{3}/3)d$ in the single M chains again gives $c = \sqrt{6}d$ (equation 5) and $s = (3\sqrt{2}/2)d$ (equation 3), but now $s = h$ instead of $2h$ for dumortierite. The result is

$$\frac{a}{c} = \frac{3}{2} + \frac{\sqrt{2}}{3} \approx 1.971 \quad (13)$$

Average ratios from 21 published sets of LLM unit-cell parameters (Ibers & Smith 1964, Klevstova & Magarill 1970, Klevstova *et al.* 1979, Ozima *et al.* 1977, Hughes *et al.* 1987, Szillat & Müller-Buschbaum 1995, Sedello

& Müller-Buschbaum 1996, Wang *et al.* 1996, 1997, 2000, Sebastian *et al.* 2003, Pless *et al.* 2006, Smit *et al.* 2006a, 2006b, 2008) are $b/a \approx 1.68$, $a/c \approx 2.07$. Although this model correctly predicts a/c lower for LLMs than DLMs (predicted 2.443, average ~ 2.5), it does not explain why b/a is significantly lower than in DLMs (average for orthorhombic structures, 1.713).

Ozima *et al.* (1977) discussed structural topological aspects of the lyonsite structure and proposed an alternative way of deriving the structure from a modified spherical close-packing. Figure 11 shows a net derived from the $\{3^3\cdot4^2\}$ semi-regular tiling of squares and equilateral triangles. Each vertex in the net is the position of an oxygen atom in one layer, and all solid edges have a unit length corresponding to the average close-packed oxygen-oxygen distance (~ 2.8 Å); the dashed edges represent slight distortions of the triangles from regularity, with lengths $[13/3 - 2\sqrt{3}]^{1/2} \approx 0.932$ and $[7/3 - 2/\sqrt{3}]^{1/2} \approx 1.086$ units each. The next layer of oxygen atoms is identical to the first shifted along a displacement vector of $1/2\mathbf{a} + 1/2\mathbf{b}$ (where \mathbf{a} , \mathbf{b} are the orthorhombic unit-cell vectors), with atoms sitting in the hollows of the first layer. Subsequent layers are stacked in an identical way. Voids created in this stacking correspond to the T^h , X , M^O , and M^P cation sites. Expanding the O–O distance slightly so that atomic spheres no longer touch (*i.e.*, transforming the close packing into an open packing) preserves the symmetry of the net and allowed Ozima *et al.* (1977) to calculate approximate bond-lengths. The b/a ratio calculated for the net in Figure 11 is

$$\frac{b}{a} = 8 - \frac{11}{\sqrt{3}} \approx 1.649 \quad (14)$$

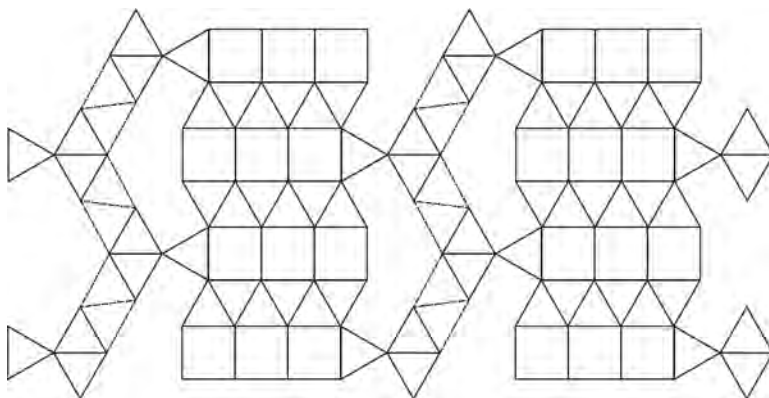


FIG. 11. Close-packed net from which Ozima *et al.* (1977) derived the lyonsite structure. Oxygen atoms sit at the vertices, and successive layers are displaced along the vector $1/2\mathbf{a} + 1/2\mathbf{b}$. Solid edges have a unit length corresponding to the distance between the centers of close-packed spheres (~ 2.8 Å for oxygen), and dashed edges indicate triangles distorted from regularity.

The estimate for c from equation 5 is still applicable if recast in terms of the edge length of the octahedron (= one O–O distance), so a/c becomes

$$\frac{a}{c} = 1 + \frac{2}{\sqrt{3}} \approx 2.154 \quad (15)$$

In reality, we find the average values for the LLM unit-cell parameter ratios lie almost exactly midway between the estimates derived from these two geometrical models. More importantly, the net of Ozima *et al.* (1977) successfully explains the departure of the lyonsite structure from the hexagonality of the {6·4·3·4} net. A similar model should be able to explain the orthorhombic dumortierite structure, but this model is not obvious.

Despite the diverse compositions that have been synthesized with the lyonsite structure, lyonsite itself has not been produced synthetically (Smit *et al.* 2006a); laboratory synthesis has always resulted in the triclinic β - $\text{Cu}_3\text{Fe}_4(\text{VO}_4)_6$, isostructural (Lafontaine *et al.* 1994) with howardevansite, which occurs at the same locality. The β phase is less closely packed and has lower coordination of both cations and anions (Wang *et al.* 2000), hence it is less dense than the α phase (3.97 g/cm³ versus 4.21 g/cm³). The lyonsite structure is also considerably denser than the dumortierite structure; replacing double-chains with single chains and reducing the size of the triangular channels leads to smaller average unit-cells.

The Satterlyite-Holtedahllite Structure

Satterlyite, ideally $\text{Fe}_{12}(\text{OH},\text{O})_6(\text{PO}_3\text{OH},\text{PO}_4)(\text{PO}_4)_5$ (Mandarino *et al.* 1978, Kolitsch *et al.* 2002), and isostructural holtedahllite, $\text{Mg}_{12}(\text{OH},\text{O})_6(\text{PO}_3\text{OH},\text{PO}_4,\text{CO}_3)(\text{PO}_4)_5$ (Raade & Mladeck 1979, Rømming & Raade 1989) possess a structure, which we will refer to as the satterlyite-holtedahllite structure, based on chains of face-sharing dimers of octahedra like the M^H chains in the dumortierite structure (Fig. 12). Bundles of three M^H -type double-chains share corners to form a triangular channel containing $T^h\Theta'_3\theta'$ tetrahedral groups just as in the hexagonal version of the dumortierite structure. These bundles can be bound by trigonally symmetric hexagonal supertiles (Fig. 13). In hexagonal DLMs, the supertiles contain three squares and one equilateral triangle, giving them two side lengths in a ratio of $\sqrt{3}:1$ which alternate around the perimeter. To form the {6·4·3·4} tiling, the supertiles share corners, leaving triangular gaps (Fig. 13A). In satterlyite and holtedahllite, the supertiles become equilateral hexagons due to distortion of the squares (which contain the M^H chains) to quadrilaterals. The supertiles fill the plane without gaps by sharing edges, forming a pattern of quadrilaterals, equilateral triangles and obtuse isosceles triangles with plane-group symmetry $p31m$ (Fig. 13B). The full (2+1)-dimensional structure has space group $P31m$.

The squares are transformed into quadrilaterals by the distortion of alternate pairs of M^H octahedra, stretching one very long (Mg,Fe)–O bond to 2.32 to 2.35 Å (the other five bonds in the same octahe-

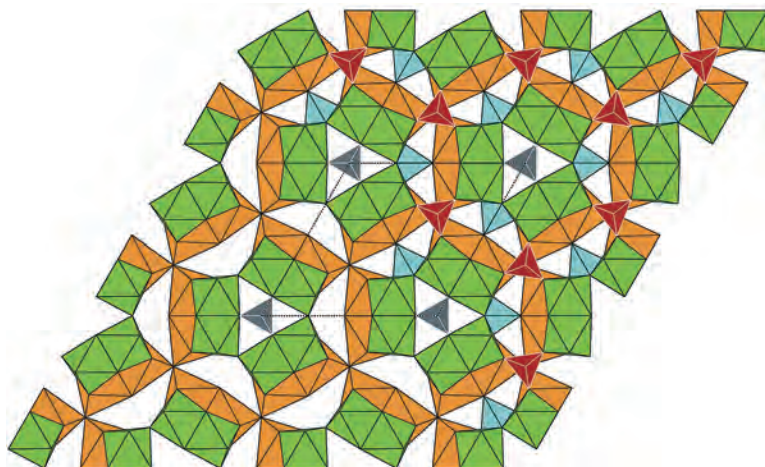


FIG. 12. Structure of satterlyite and holtedahllite (based on the structure from Rømming & Raade 1989) viewed down the c -axis (space group $P31m$). The M^{H1} , M^{H2} octahedra are shown in green and orange, respectively, T^h tetrahedra in grey, T^h tetrahedra in blue and T^h tetrahedra in red; T^h and T^h tetrahedra are hidden in the lower left half of the figure to display the M^{H1} , M^{H2} double-chains. The dotted black line shows the unit cell.

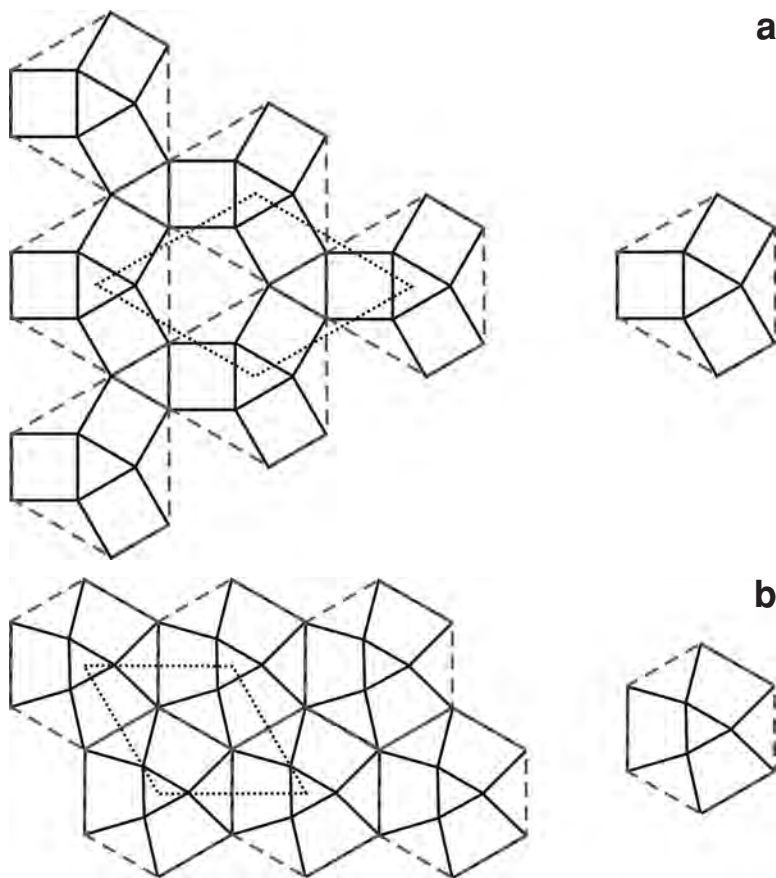


FIG. 13. The (A) ellenbergerite and (B) satterlyite-holtedahlite structures (viewed down their respective c -axes) contain triangular channels formed by bundles of three M^H double-chains of octahedra. Dashed lines show how each structure (left) can be assembled from hexagonal supertiles (right) containing the bundles. The satterlyite-holtedahlite tile is equilateral, creating a distortion in the chains of octahedra. Two-dimensional unit cells are shown as dotted lines.

dron average 2.095 Å in holtedahlite and 2.154 Å in satterlyite; the other octahedrally coordinated site has average bond-length 2.076 Å in holtedahlite and 2.119 Å in satterlyite; Rømming & Raade (1989), Kolitsch *et al.* (2002)). The satterlyite-holtedahlite M^H chain contains two cation sites that are crystallographically and topologically distinct: the distorted M^{H1} site (orange in Fig. 13) and the less-distorted M^{H2} site (green in Fig. 12), and two corresponding 4-coordinate anions, Φ^{H1} and Φ^{H2} , completely internal to the double-chain (the Φ^{H1} and Φ^{H2} are not topologically distinct, but it is still convenient to distinguish them in the structure-generating function). There are six of each octahedrally coordinated site per unit cell (see Fig. 12).

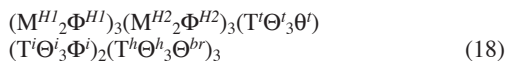
There are three separate tetrahedral groups in the satterlyite-holtedahlite structure. The $T^i\Theta^j\theta^k$ groups (grey in Fig. 12) are unchanged in symmetry or topology from the DLM structure; there is one per unit cell.

A second tetrahedral group (blue in Fig. 12) nestles in the corners between M^H chains, similar to the $T^h\Theta^h_3\theta^h$ groups in the dumortierite structure. However, the apex of this tetrahedron is not in a hexagonal channel but on a 3-coordinate oxygen site in another M^H chain (where an additional Θ^i is found in the dumortierite structure). We designate this bridging anion as Θ^{br} and write the group as $T^h\Theta^h_3\Theta^{br}$. There are three of these groups per unit cell.

The distorted vertex on the M^{H1} site is shared by three M^{H1} octahedra in separate chains and sits on a threefold symmetry axis. Above sit three vertices on M^{H2} octahedra in the three chains (which would coordinate additional T^h sites in dumortierite). These four vertices create an interstitial tetrahedrally coordinated site, T^i (red in Fig. 12); the distorted vertex is therefore 4-coordinated. We write this final tetrahedral group as $T^i\Theta^i\Phi^i$, and there are two per unit cell. The topological difference between the coordinations of the M^{H1} and M^{H2} cations is now apparent: M^{H2} is coordinated by four 3-coordinate ($2 \times \Theta^h, \Theta^i, \Theta^j$) and two 4-coordinate (Φ^{H1}, Φ^{H2}) anions, the same as M^H in DLMs, but M^{H1} is coordinated by three 3-coordinate ($\Theta^{br}, \Theta^h, \Theta^j$) and three 4-coordinate ($\Phi^{H1}, \Phi^{H2}, \Phi^i$) anions.

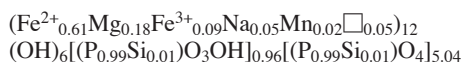
Both T^i and T^j tetrahedra are oriented in the same direction, *i.e.*, with $T^i-\Theta^i$ and $T^i-\Phi^i$ bonds pointing up the *c*-axis. Where the T^h orientation is defined as above for the DLM T^h groups, they also point up. There is no evidence in satterlyite or holtedahlite for downward-pointing $T^i\Theta^i\Phi^i$ tetrahedra or apex-sharing $T^j_2\Theta^j_6\theta^j$ groups in the triangular channels.

In deriving the satterlyite-holtedahlite structure from elements of the dumortierite structure, we have constructed its structure-generating function:



As in the case of the lyonsite structure, a more rigorous derivation by the partitioning of local cation environments arrives at the same result as our more heuristic approach.

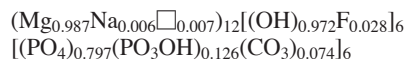
Satterlyite is a yellow to brown mineral found in nodules in shales at Big Fish River, Yukon, Canada (Mandarino *et al.* 1978). Its empirical composition is equivalent to



with maximum SiO_2 content approximately 0.2 wt.% (Mandarino *et al.* 1978). Infrared spectroscopy shows no CO_3^{2-} groups present. Kolitsch *et al.* (2002) found that the larger Fe^{2+} cation has a slight preference for the larger, more distorted M^H octahedron, with approximately $\text{Fe}_{0.84}\text{Mg}_{0.16}$ at M^{H1} and $\text{Fe}_{0.71}\text{Mg}_{0.29}$ at M^{H2} . The authors conjectured that a minimum amount of Mg may be necessary to stabilize the structure. Optical absorption spectroscopy suggests Fe^{2+} is at a more distorted site than Fe^{3+} , *i.e.*, Fe^{3+} may prefer M^{H2} , and EPR spectroscopy confirms the presence of small amounts of Mn^{2+} (Chandrasekhar *et al.* 2003). The structure was determined by Y. Le Page but was not published (Rømming & Raade 1989, Kolitsch *et al.* 2002).

Holtedahlite occurs at the Tingelstjertn quarry, Modum, Norway (Raade & Mladeck 1979) and Gole Gohar, Bafq district, Iran (Mücke & Younessi 1994),

and is colorless or greyish from inclusions of magnetite. At Modum, where it occurs with carbonate-bearing phosphoellenbergerite, its empirical composition is equivalent to



plus an additional 0.06 wt.% MnO. Carbonate groups substitute for phosphate as the $T^i\Theta^i\theta^i$ groups in the triangular channel (Rømming & Raade 1989), similar to phosphoellenbergerite from the same locality. At both localities, holtedahlite may contain up to 2-4 wt.% SiO_2 , 0.2-0.8 wt.% SO_3 , and 0.05-0.4 wt.% Na_2O (Brunet *et al.* 1998). Synthetic holtedahlite $[\text{Mg}_2(\text{OH},\text{O})_6(\text{PO}_3\text{OH},\text{PO}_4)(\text{PO}_4)_5]$ has also been produced by hydrothermal synthesis (Rømming & Raade 1989, Raade 1990, Brunet *et al.* 1998). No other materials with the satterlyite-holtedahlite structure have been synthesized. Holtedahlite has slightly smaller unit-cell parameters than satterlyite ($a = 4.977$, $c = 11.203$ Å for naturally occurring holtedahlite; $a = 5.039$, $c = 11.355$ Å for satterlyite) commensurate with the larger cation radius of Fe^{2+} versus Mg.

Bond-valence analysis (Rømming & Raade 1989, Kolitsch *et al.* 2002), infrared (Rømming & Raade 1989, Brunet & Schaller 1996), and NMR spectroscopy (Brunet & Schaller 1996) suggest that OH occupies analogous positions to those in DLMs, at Φ^{H1} , Φ^{H2} , and θ^i . However, charge-balance requirements mean that all three H sites cannot be fully occupied, hence H is disordered in the structure. On the basis of $\text{OH}\cdots\text{O}$ distances of 3.0 to 3.2 Å from IR (Raade & Mladeck 1979, Rømming & Raade 1989, Brunet & Schaller 1996), hydrogen bonding in the structure is weak.

Bond valence also indicates that the distorted vertex of the M^{H1} octahedron, the 4-coordinate Φ^i , has low incident bond-valence: around 1.69 valence units (Rømming & Raade 1989, Kolitsch *et al.* 2002). Rømming & Raade (1989) found that bond-lengths involving Φ^i show significant differences between naturally occurring and synthetic holtedahlite: $T^i(\text{P})-\Phi^i$ is shorter (1.549 Å synthetic, 1.592 Å natural) and $M^{H1}(\text{Mg})-\Phi^i$ longer (2.361 Å synthetic, 2.324 Å natural) in carbonate-free synthetic holtedahlite versus naturally-occurring holtedahlite. Satterlyite, which also is carbonate-free, has $T^i-\Phi^i$ and $M^{H1}-\Phi^i$ bond lengths that resemble synthetic holtedahlite, 1.555 and 2.359 Å, respectively (Kolitsch *et al.* 2002). The Φ^i anion has a higher anisotropy than most others in the structure (the exception is 1-coordinate θ^j); $U_{11/22}$ and U_{33} for Φ^i are nearly equal in naturally occurring holtedahlite, whereas in synthetic holtedahlite and satterlyite, U_{33} is less than $1/3 U_{11/22}$ (Rømming & Raade 1989, Kolitsch *et al.* 2002). A small amount of OH may substitute at the Φ^i position, as suggested by Kolitsch *et al.* (2002), locally lengthening the $T^i-\Phi^i$ bond and shortening the $M^{H1}-\Phi^i$ bond. This small amount may increase with

carbonate substitution at $T^i\Theta^j\Phi^k$, thus increasing both the average $T^i-\Phi^k$ bond length and disorder in the c -axis direction. However, Brunet & Schaller (1996) could detect no evidence of OH in the $T^i\Theta^j\Phi^k$ group via IR or NMR; Rømming & Raade (1989) conjectured that the low bond-valence total of Φ^k is due to inadequacies of bond-valence functions in modeling long Mg–O bonds.

Endmember holtedahlite is one of several polymorphs of Mg_2PO_4OH (Raade 1990); another, althausite, also has Modum, Norway, as its type locality. Raade (1990) and Brunet *et al.* (1998) found that holtedahlite is favored at low temperature (below 600 °C) and intermediate pressure (~5–10 kbar), whereas althausite is favored at higher temperature and lower pressure. Brunet *et al.* (1998) found that where the two polymorphs occur together at Modum, small amounts of Si, S, C, and Na are partitioned into holtedahlite, whereas F is partitioned into althausite; they suggested that the counteracting stabilization effects of these minor substituents allow the coexistence of holtedahlite and althausite over a wider range of temperature and pressure. Larger amounts of F stabilize wagnerite, Mg_2PO_4F , over both minerals (Brunet *et al.* 1998); the ferrous analogue of wagnerite, wolfeite, occurs with satterlyite at Big Fish River (Mandarino *et al.* 1978).

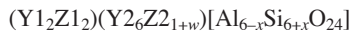
The cancrinite-AB Structure

The cancrinite group of minerals (Deer *et al.* 2004, Bonaccorsi & Merlino 2005, Pekov *et al.* 2011) are feldspathoids with tectoaluminosilicate frameworks consisting of layers of six-membered rings of tetrahedra perpendicular to the c -axis. Each layer has rings centered on three- or sixfold axes at $(1/3, 2/3, z)$ (type A), $(2/3, 1/3, z)$ (type B), or $(0, 0, z)$ (type C). The simplest stacking sequence without adjacent repeats is the two-layer ...ABABAB... repeat sequence, which we will refer to as the cancrinite-AB structure. More complex stacking sequences are known with up to 36 layers (*cf.* Smith 1988, Deer *et al.* 2004, Bonaccorsi & Merlino 2005, Cámara *et al.* 2012).

The framework created by the AB stacking contains wide channels bound by twelve-membered rings of tetrahedra and narrower channels bound by six-membered rings. Various extra-framework ions (both “point” cations such as Na^+ or Ca^{2+} , and anion groups such as CO_3^{2-} , PO_4^{3-} , or $C_2O_4^{2-}$) occupy certain positions inside these channels. Tecto(alumino)silicate structures are usually simplified by representing each tetrahedron by a node and each (Si,Al)–O–(Si,Al) connection by an edge, reducing the structure to a graph on a three-dimensional lattice. Using this representation, the narrow channel becomes a stack of polyhedral cages called cancrinite or $[4^6 6^3 6^2]$ cages (Smith 1988). The latter notation derives from the eleven faces of the cage; two parallel hexagonal faces are joined by pairs of quadrilateral faces alternating with non-planar hexagonal faces (Fig. 14B). The cages stack by sharing

the parallel hexagonal faces such that the narrow channels are lined by zigzag ribbons of quadrilateral faces and ribbons of hexagonal faces. Each stack of cages (*i.e.*, each narrow channel) contains nodes from either the A layers or the B layers, but not both; A stacks join B stacks by sharing quadrilateral faces, and the wide channels (lined by non-planar hexagonal faces alone) are gaps created by rings of six stacks. By once again replacing nodes in the ribbons of quadrilateral faces with tetrahedra, we obtain double-chains of tetrahedra. If instead each node is replaced by an octahedron, we obtain M^h -type double-chains of octahedra, and the entire framework becomes the framework of the dumortierite structure with hexagonal symmetry (*i.e.*, the ellenbergerite structure). The underlying cation-only lattices of the cancrinite-AB and the hexagonal DLM frameworks are topologically identical. In addition, the extra-framework ions in most cancrinite-AB structures occupy positions analogous to T^h and X in the wide channel and T^i in the narrow channel.

The structure of cancrinite (Fig. 14A) was first solved by Jarchow (1965). Eleven minerals of the cancrinite group have the AB stacking sequence, including cancrinite itself; their detailed structures and chemical compositions are described in Deer *et al.* (2004), Bonaccorsi & Merlino (2005), and Pekov *et al.* (2011). Their general composition can be described approximately by



where Y1, Z1 represent cations and anions in the narrow channel (*i.e.*, in the cancrinite cages), at positions analogous to the T^i sites in DLMs; Y2 represents cations in the wide channel, at positions analogous to the T^h sites; and Z2 represents anions in the wide channel, at positions analogous to the X sites ($w = 0$ to 1). The framework is given by $[Al_{6-x}Si_{6+x}O_{24}]$; in almost every cancrinite-AB mineral, the Si and Al positions are ordered (resulting in space group $P6_3$ or $P6_3/m$) and Si:Al = 1:1, but cancrisilite is disordered ($P6_3mc$) with ideally Si:Al = 7:5. Cancrinite itself is ideally $Na_7Ca[Al_6Si_6O_{24}](CO_3)_{1.5}\cdot 2H_2O$ (Pekov *et al.* 2011).

A diverse group of cations and anions occur at the extra-framework sites. The contents of the narrow channel are usually either $Na_2(H_2O)_2$ as in cancrinite or Ca_2Cl_2 as in davynite (Pekov *et al.* 2011). Cations in the wide channel are usually occupied by Na^+ , K^+ , Ca^{2+} , or \square , and anion sites can be occupied by CO_3^{2-} , SO_4^{2-} , OH^- , S^{2-} , Cl^- , PO_4^{3-} , $C_2O_4^{2-}$, \square , or others. Some minerals also have H_2O sites in the wide channels with no hexagonal-channel analogues in the dumortierite structure.

The minimal cancrinite-AB unit-cell parameters lie in the ranges 5.1–5.4 Å for c and 12.55–12.85 Å for a . This leads to a/c ratios of around 2.45 for minerals with $Na_2(H_2O)_2$ in the narrow channel, and around 2.39 for those with Ca_2Cl_2 . Ordering of extra-framework ions

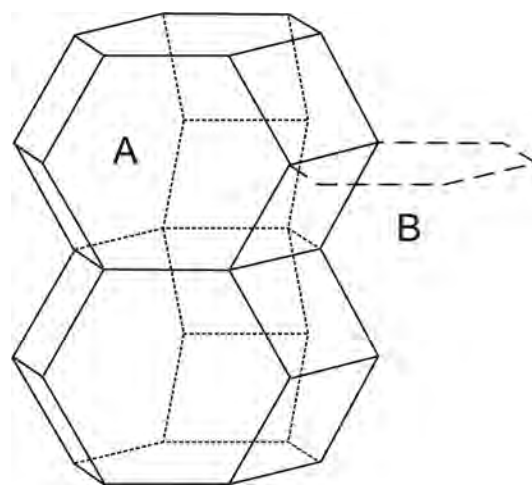
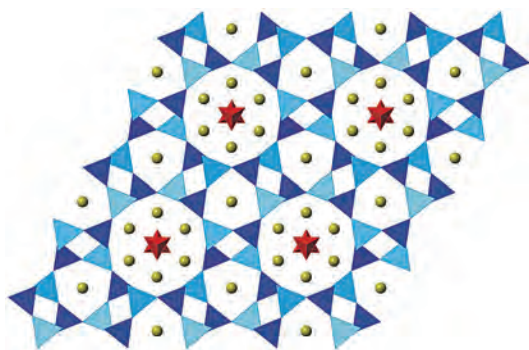


FIG. 14. (A) Crystal structure of cancrinite (based on structure data from Hassan *et al.* 2006). The Si,Al tetrahedra are blue; CO_3^{2-} groups are red; yellow spheres are Na^+ or H_2O . (B) Stacked $[4^6 6^3]$ cancrinite cages, after Smith (1988). The full cages belong to the A layers, with the position of an adjacent cage belonging to the B layers indicated.

between the wide channels can increase the unit cell, multiplying a by $\sqrt{3}$ as in microsommite and pitiglianoite or by 2 as in quadridavnye (Bonaccorsi & Merlino 2005, Pekov *et al.* 2011).

In addition to the cancrinite-group aluminosilicates, the beryllophosphate tiptopite, $\text{K}_2(\text{Li}_{2.9}\text{Na}_{1.7}\text{Ca}_{0.7}\square_{0.7})_{\Sigma 6}[\text{Be}_6\text{P}_6\text{O}_{24}](\text{OH})_2 \cdot 1.3\text{H}_2\text{O}$, also has the cancrinite-AB structure, with $a = 11.655$, $c = 4.692$ Å ($alc = 2.484$) and space group $P6_3$ (Peacor *et al.* 1987). Its framework is $[\text{Be}_6\text{P}_6\text{O}_{24}]$, with Be and P ordered. The narrow channel contains $\square_2\text{K}_2$, with Li^+ , Na^+ , Ca^{2+} , OH^- , and H_2O in the wide channel. Many synthetic materials with the cancrinite-AB structure are also known, and are summarized in Table 1 of Sirbescu & Jenkins (1999) and Table 3 of Bonaccorsi & Merlino (2005). They include structures with the frameworks $[\text{Al}_6\text{Ge}_6\text{O}_{24}]$, $[\text{Ga}_6\text{Ge}_6\text{O}_{24}]$, $[\text{Zn}_6\text{P}_6\text{O}_{24}]$, and $[\text{Co}_6\text{P}_6\text{O}_{24}]$, as well as several exotic extra-framework ions.

Comparison of structures

The lyonsite, satterlyite-holtedahlite and cancrinite-AB structures each show similarities to the dumortierite and ellenbergerite structures in different ways, and these similarities highlight different aspects of the structure. The lyonsite structure, like the dumortierite structure, is based on a framework of chains of 6-coordinate sites assembled into the $\{6\cdot 4\cdot 3\cdot 4\}$ net, with the same “bracelet and pinwheel” structure in the hexagonal channels; however, the double-chains of octahedra are replaced by single chains of octahedra and triangular prisms, and the triangular channels are empty. Like the dumortierite structure, the lyonsite structure contains two types of framework chains in 2:1 proportion, altering the hexagonal structure to an orthorhombic one with space-group symmetry $Pm\bar{c}n$. The satterlyite-

holtedahlite structure contains the same bundles of three corner-sharing zigzag chains of face-sharing dimers of octahedra around a triangular channel as the ellenbergerite structure, but assembled in a different way. The cancrinite-AB structure is based on a framework of tetrahedra that, where tetrahedra are replaced by octahedra, gives the ellenbergerite framework. Both structures also have additional elements at similar positions in their open channels: positions of the extra-framework ions in the cancrinite-AB structure correspond to the tetrahedrally and octahedrally coordinated sites inside the triangular and hexagonal channels in the ellenbergerite structure. In other words, the cancrinite-AB and ellenbergerite structures are based on similar underlying lattices. Finally, the orthorhombic dumortierite and hexagonal ellenbergerite structures, although geometrically and topologically similar in many ways, themselves differ not only in symmetry, but also in how they are constructed from slabs of slightly different geometric elements (Fig. 4).

These comparisons all feature different ways of (dis)assembling the DLM structure; as geometrical elements combined in different ways, as designs on different tilings, as connectivity graphs on an underlying lattice, or as done by Ozima *et al.* (1977) for lyonsite, as a close-packed layers of anions. Each of these decompositions highlight different features of the parent structure, and lead to different ways of generalizing the structure and recognizing commonalities with other structures. The structure-generating function is one way of describing some of these commonalities in a formula that contains both chemical and topological information about a structure or class of structures. It suggests the possibility of treating classes of crystal structures algebraically.

These types of in-depth descriptive studies of crystal structures touch on many seemingly abstract mathematical ideas from geometry, group theory, topology, and graph theory. The geometrical and topological similarities among different structures, and among isostructural materials, can go far beyond chemistry, as the diverse compositions of the dumortierite-like materials, lyonsite-like materials, and materials with the cancrinite-AB structure demonstrate. Understanding the geometrical and topological natures of crystal structures is an important step in answering the deeper questions of why materials assume the structures that they do.

ACKNOWLEDGEMENTS

The authors thank Robert Martin, Joel Grice, and Frank Hawthorne for their comments. Financial support was provided by the Natural Sciences and Engineering Research Council of Canada in the form of a Discovery Grant to LAG.

REFERENCES

- ALEXANDER, V.D., GRIFFEN, D.T., & MARTIN, T.J. (1986) Crystal chemistry of some Fe- and Ti-poor dumortierites. *American Mineralogist* **71**, 786-794.
- AMORÓS, P., MARCOS, M.D., ROCA, M., BELTRÁN-PORTER, A., & BELTRÁN-PORTER, D. (1996) Synthetic pathways for new tubular transition metal hydroxy- and fluoroselenites: crystal structures of $M_{12}(X)_2(SeO_3)_8(OH)_6$ ($M = Co^{2+}, Ni^{2+}; X = OH^-$). *Journal of Solid State Chemistry* **126**, 169-176.
- APPLIN, K.R. & HICKS, B.D. (1987) Fibers of dumortierite in quartz. *American Mineralogist* **72**, 170-172.
- ATTFIELD, M.P., MORRIS, R.E., & CHEETHAM, A.K. (1994) Synthesis and structures of two isostructural phosphites, $Fe_{11}(HPO_3)_8(OH)_6$ and $Mn_{11}(HPO_3)_8(OH)_6$. *Acta Crystallographica* **C50**, 981-984.
- BELLER, U. (1987) Hochdruck-Synthese von phosphorhaltigem Ellenbergerit. Diplomarbeit, Ruhr-Universität Bochum, Bochum, Germany.
- BEUKES, G.J., SLABBERT, M.J., DE BRUIYN, H., BOTHA, B.J.V., SCHOCH, A.E., & VAN DER WESTHUIZEN, W.A. (1987) Tidumortierite from the Keimoes area, Namaqua mobile belt, South Africa. *Neues Jahrbuch für Mineralogie (Abhandlungen)* **157**, 303-318.
- BONACCORSI, E. & MERLINO, S. (2005) Modular microporous minerals: cancrinite-davyne group and C-S-H phases. *Reviews in Mineralogy and Geochemistry* **57**, 241-290.
- BORGHİ, A., COSSIO, R., FIORA, L., OLMI, F., & VAGGELLI, G. (2004) Chemical determination of coloured zoned minerals in 'natural stones' by EDS/WDS electron microprobe: an example from dumortierite quartzites. *X-ray Spectrometry* **33**, 21-27.
- BRUNET, F. & SCHALLER, T. (1996) Protons in the magnesium phosphates phosphoellenbergerite and holtedahlite: An IR and NMR study. *American Mineralogist* **81**, 385-394.
- BRUNET, F., CHOPIN, C., & SEIFERT, F. (1998) Phase relations in the $MgO-P_2O_5-H_2O$ system and the stability of phosphoellenbergerite: petrological implications. *Contributions to Mineralogy and Petrology* **131**, 54-70.
- CÁMARA, F., BELLATRECCIA, F., DELLA VENTURA, G., GUNTER, M. E., SEBASTIANI, M., & CAVALLO, A. (2012) Kircherite, a new mineral of the cancrinite-sodalite group with a 36-layer stacking sequence: Occurrence and crystal structure. *American Mineralogist* **97**, 1494-1504.
- CEMPÍREK, J. & NOVÁK, M. (2004) Dumortierite and tourmaline from abyssal pegmatites from Vémyslice near Moravský Krumlov, Gföhl unit, Moldanubicum. *Acta Musei Moraviae, Scientiae Geologicae* **89**, 45-54 (in Czech with English abstract).
- CEMPÍREK, J. & NOVÁK, M. (2005) A green dumortierite from Kutná Hora region, Czech Republic: spectroscopic and structural study. In International meeting: Crystallization Processes in Granitic Pegmatites, Elba, Italy (F. Pezzotta, ed.). 4-5.
- CEMPÍREK, J., NOVÁK, M., DOLNÍČEK, Z., KOTKOVÁ, J., & ŠKODA, R. (2010) Crystal chemistry and origin of grandierite, ominelite, boralsilite, and wendingite from the Bory Granulite Massif, Czech Republic. *American Mineralogist* **95**, 1533-1547.
- CHANDRASEKHAR, A.V., VENKATA RAMANAIHAH, M., REDDY, B.J., REDDY, Y.P., RAO, P.S., & RAVIKUMAR R.V.S.S.N. (2003) Optical and EPR studies of iron bearing phosphate minerals: satterlyite and gormanite from Yukon Territory, Canada. *Spectrochimica Acta A* **59**, 2115-2121.
- CHE, R.C., PENG, L.-M., & ZHOU, W. Z. (2005) Synthesis and characterization of crystalline microporous cobalt phosphite nanowires. *Applied Physics Letters* **87**, 173122.
- CHOO, C.O. & KIM, Y. (2001) Mineralogical studies of dumortierite from the Miryang clay deposit, Korea. *Geosciences Journal* **5**, 273-279.
- CHOO, C.O. & KIM, Y. (2003) Textural and spectroscopic studies on hydrothermal dumortierite from an Al-rich clay deposit, southeastern Korea. *Mineralogical Magazine* **67**, 799-806.
- CHOPIN, C., FERRARIS, G., IVALDI, G., SCHERTL, H.P., SCHREYER, W., COMPAGNONI, R., DAVIDSON, C., & DAVIS, A.M. (1995) Magnesiodumortierite, a new mineral from very-high-pressure rocks (Western Alps). Part II: Crystal chemistry and petrological significance. *European Journal of Mineralogy* **7**, 525-535.
- CHOPIN, C., KLASKA, R., MEDENBACH, O., & DRON, D. (1986) Ellenbergerite, a new high-pressure Mg-Al-(Ti,Zr)-silicate with a novel structure based on face-sharing octahedra. *Contributions to Mineralogy and Petrology* **92**, 316-321.

- CHOPIN, C. & LANGER, K. (1988) Fe²⁺-Ti⁴⁺ charge-transfer between face-sharing octahedra: polarized absorption spectra and crystal chemistry of ellenbergerite. *Bulletin de Minéralogie* **111**, 17-27.
- CHOPIN, C., LANGER, K., & KHOMENKO, V. (2009) Fe²⁺-Ti⁴⁺ vs. Fe²⁺-Fe³⁺ charge transfer and short range order in single chains of face-sharing octahedra: ellenbergerite and dumortierite. *Geophysical Research Abstracts* **11**, EGU2009-9087-2.
- CHOPIN, C., SCHREYER, W., & BALLER, T. (1992) Ellenbergerite stability: A reappraisal. *Terra Nova Abstract Supplement* **1**, 10.
- CHOPIN, C. & SOBOLEV, N.V. (1995) Principal mineralogic indicators of UHP in crustal rocks. In *Ultra-high-pressure metamorphism* (R.G. Coleman and X. Wang, eds). Cambridge University Press, Cambridge, (97-131).
- CLARINGBULL, G. F. & HEY, M. H. (1958) New data for dumortierite. *Mineralogical Magazine* **21**, 901-907.
- COMODI, P. & ZANAZZI, P. F. (1993a) Structural study of ellenbergerite. Part I: Effects of high temperature. *European Journal of Mineralogy* **5**, 819-829.
- COMODI, P. & ZANAZZI, P. F. (1993b) Structural study of ellenbergerite. Part II: Effects of high pressure. *European Journal of Mineralogy* **5**, 831-838.
- DEER, W.A., HOWIE, R.A., WISE, W.S., & ZUSSMAN, J. (2004) *Rock-forming minerals. Vol. 4B Second Edition. Framework silicates: silica minerals, feldspathoids and the zeolites*. The Geological Society, London, 369-386.
- DOBEVIĆ, T., KARANOVIĆ, L.J., & TILLMANN, E. (2008) Structural and spectroscopic study of Mg_{13.4}(OH)₆(HVO₄)₂(H_{0.2}VO₄)₆. *Crystal Research and Technology* **43**, 1202-1209.
- EVANS, R.J., FYFE, C.A., GROAT, L.A., & LAM, A. E. (2012) MAS NMR measurements and ab initio calculations of the ²⁹Si chemical shifts in dumortierite and holtite. *American Mineralogist* **97**, 329-340.
- FARGES, F., GALOISY, L., BALAN, E., FUCHS, Y., & LINARÈS, J. (2004) Structure and color of the Jack Creek dumortierite (Montana, USA) using spectroscopic approaches. *Mitteilungen der Österreichischen Mineralogischen Gesellschaft* **149**, 29.
- FERRARIS, G., IVALDI, G., & CHOPIN, C. (1995) Magnesiodumortierite, a new mineral from very-high-pressure rocks (Western Alps). Part I: Crystal structure. *European Journal of Mineralogy* **7**, 167-174.
- FUCHS, Y., ERTL, A., HUGHES, J.M., PROWATKE, S., BRANDSTÄTTER, F., & SCHUSTER, R. (2005) Dumortierite from the Gföhl unit, Lower Austria: chemistry, structure, and infra-red spectroscopy. *European Journal of Mineralogy* **17**, 173-183.
- GALLISKI, M.A., MÁRQUEZ-ZAVALÍA, M.F., LIRA, R., CEMPÍREK, J., & ŠKODA, R. (2012) Mineralogy and origin of the dumortierite-bearing pegmatites of Virorco, San Luis, Argentina. *Canadian Mineralogist* **50**, 873-894.
- GOLOVASTIKOV, N.I. (1965) The crystal structure of dumortierite. *Soviet Physics-Doklady* **10**, 493-495.
- GOREVA, J.S., MA, C., & ROSSMAN, G.R. (2001) Fibrous nano-inclusions in massive rose quartz: The origin of rose coloration. *American Mineralogist* **86**, 466-472.
- GREW, E.S. (1996) Borosilicates (exclusive of tourmaline) and boron in rock-forming minerals in metamorphic environments. In *Boron: Mineralogy, Petrology, and Geochemistry* (E.S. Grew & L.M. Anovitz, eds.). Reviews in Mineralogy, Mineralogical Society of America, Washington, D.C. 862pp.
- GROAT, L.A., GREW, E.S., ERCIT, T.S., & PIECZKA, A. (2001) The crystal chemistry of dumortierite and holtite, aluminoborosilicates with heavy elements. *Geological Society of America Abstracts with Programs* **33**, Abstract 383.
- GROAT, L.A., EVANS, R.J., GREW, E.S., PIECZKA, A., & ERCIT, T.S. (2009) The crystal chemistry of holtite. *Mineralogical Magazine* **73**, 1033-1050.
- GROAT, L.A., EVANS, R.J., GREW, E.S., & PIECZKA, A. (2012) Crystal chemistry of As- and Sb-bearing dumortierite. *Canadian Mineralogist* **50**, 855-872.
- GU, Z., ZHAI, T., GAO, B., ZHANG, G., KE, D., MA, Y., & YAO, J. (2007) Controlled hydrothermal synthesis of nickel phosphite nanocrystals with hierarchical superstructures. *Crystal Growth & Design* **7**, 825-830.
- HASSAN, I., ANTAO, S.M., & PARISE, J.B. (2006) Cancrinite: Crystal structure, phase transitions and dehydration behavior with temperature. *American Mineralogist* **91**, 1117-1124.
- HAWTHORNE, F.C. (2010) Generating functions for structure and chemical composition. *Acta Mineralogica-Petrographica Abstract Series* **6**, 734.
- HOSKINS, B.F., MUMME, W.G., & PRYCE, M.W. (1989) Holtite, (Si_{12.25}Sb_{0.75})B|(Al₁₆(Al_{0.43}Ta_{0.27}□_{0.30})O₁₅(O,OH)_{2.25}): crystal structure and crystal chemistry. *Mineralogical Magazine* **53**, 457-463.
- HU, T., LIN, J.B., KONG, F., & MAO, J.G. (2008) Mg₇V₄O₁₆(OH)₂(H₂O): A magnesium vanadate with a novel 3D magnesium oxide open framework. *Inorganic Chemistry Communications* **11**, 1012-1014.
- HUGHES, J.M., STARKEY, S.J., MALINCONICO, M.L., & MALINCONICO, L. (1987) Lyonsite, Cu²⁺₃Fe³⁺₄(VO₄)³⁻₆, a new fumarolic sublimate from Izalco volcano, El Salvador: Descriptive mineralogy and crystal structure. *American Mineralogist* **72**, 1000-1005.

- HUGHES, R.W., GERRARD, L.A., PRICE, D.J., & WELLER, M.T. (2003) A hybrid metalloarsenate 3D framework-1D interrupted metal oxide. *Inorganic Chemistry* **42**, 4160-4164.
- IBERS, J.A. & SMITH, G.W. (1964) Crystal structure of a sodium cobalt molybdate. *Acta Crystallographica* **17**, 190-197.
- JARCHOW, O. (1965) Atomanordnung und Strukturverfeinerung von Cancrinit. *Zeitschrift für Kristallographie* **122**, 407-422.
- JEFFERY, J.A. (1943) The sillimanite group of minerals. *California Journal of Mines and Geology* **89**, 383-390.
- JIN, L., HONG, J., & NI, Y. (2010) Large-scale synthesis of $Mn_{11}(HPO_3)_8(OH)_6$ superstructures constructed by micro-rods via a mixed-solvothermal route. *Materials Chemistry and Physics* **123**, 337-342.
- KATO, K., YANKE, Y., OKA, Y., & YAO, T. (1998) Crystal structure of a zinc hydroxide sulfate vanadate(V), $Zn_7(OH)_3(SO_4)(VO_4)_3$. *Zeitschrift für Kristallographie - New Crystal Structures* **213**, 26.
- KATZ, L., KASENALLY, A., & KIHNBORG, L. (1971) The crystal structure of the reduced copper molybdate $Cu_{4-x}Mo_3O_{12}$ ($x \approx 0.15$). *Acta Crystallographica* **B27**, 2071-2077.
- KAZANTSEV, S.S., PUSHCHAROVSKY, D.YU., PASERO, M., MERLINO, S., ZUBKOVA, N.V., KABALOV, YU.K., & VOLOSHIN, A.V. (2005) Crystal structure of holtite I. *Crystallography Reports* **50**, 42-47.
- KAZANTSEV, S.S., ZUBKOVA, N.V., & VOLOSHIN, A.V. (2006) Refinement of composition and structure of holtite I. *Crystallography Reports* **51**, 412-413.
- KELLER, P. (2001) Ekatite, $(Fe^{3+}, Fe^{2+}, Zn)_{12}(OH)_6[AsO_3]_6 [AsO_3 \cdot HOSiO_3]_2$, a new mineral from Tsumeb, Namibia, and its crystal structure. *European Journal of Mineralogy* **13**, 769-777.
- KLEVTSOVA, R.F., ANTONOVA, A.A., & GLINSKAYA, L.A. (1979) Crystal structure of lithium-zirconium molybdate $Li_2Zr(MoO_4)_3$. *Kristallografiya* **24**, 596-599 (in Russian).
- KLEVTSOVA, R.F. & MAGARILL, S.A. (1970) Crystal structure of lithium-iron molybdates $Li_3Fe(MoO_4)_3$ and $Li_2Fe_2(MoO_4)_3$. *Kristallografiya* **15**, 710-715 (in Russian).
- KOLITSCH, U., ANDRUT, M., & GIESTER, G. (2002) Satterlyite, $(Fe, Mg)_{12}(PO_3OH)(PO_4)_5(OH)_6$: crystal structure and infrared absorption spectra. *European Journal of Mineralogy* **14**, 127-133.
- LAFONTAINE, M.A., GREÑEÇHE, J.M., LALIGANT, Y., & FÉREY, G. (1994) β - $Cu_3Fe_4(VO_4)_6$: structural study and relationships; physical properties. *Journal of Solid State Chemistry* **108**, 1-10.
- LIAO, K. & NI, Y. (2010) Synthesis of hierarchical $Ni_{11}(HPO_3)_8(OH)_6$ superstructures based on nanorods through a soft hydrothermal route. *Materials Research Bulletin* **45**, 205-209.
- MA, C., GOREVA, J.S., & ROSSMAN, G.R. (2002) Fibrous nano-inclusions in massive rose quartz: HRTEM and AEM investigations. *American Mineralogist* **87**, 269-276.
- MAHAPATRA, S. & CHAKRABARTY, A. (2011) Dumortierite from Susnia Hill, Bankura District, West Bengal, India. *Current Science* **100**, 299-301.
- MANDARINO, J. A., STURMAN, B. D., & CORLETT, M. I. (1978) Satterlyite, a new hydroxyl-bearing phosphate from the Big Fish River area, Yukon Territory. *Canadian Mineralogist* **16**, 411-413.
- MARCOS, M.D., AMORÓS, P., BELTRÁN, A., & BELTRÁN, D. (1993a) New tubular transition metal oxoanionic derivatives: a systematic approach to condensed phases of the dumortierite family. *Solid State Ionics* **63-65**, 87-95.
- MARCOS, M.D., AMORÓS, P., BELTRÁN-PORTER, A., MARTÍNEZ-MÁÑEZ, R., & ATTFIELD, J.P. (1993b) Novel crystalline microporous transition-metal phosphites $M_{11}(HPO_3)_8(OH)_6$ ($M = Zn, Co, Ni$). X-ray powder diffraction structure determination of the Co and Ni derivatives. *Chemistry of Materials* **5**, 121-128.
- MARCOS, M.D., AMORÓS, P., BELTRÁN, D., BELTRÁN, A., & ATTFIELD, J.P. (1995) Non-stoichiometric tubular nickel(II) hydroxyarsenates of the dumortierite family: Crystal structure and topochemical thermal reduction of $Ni_{12+x}H_{6-x}(AsO_4)_8(OH)_6$ ($x = 1.16$ and 1.33). *Journal of Materials Chemistry* **5**, 917-925.
- MARCOS, M.D., AMORÓS, P., & LE BAUL, A. (1993c) Synthesis and crystal structure of a tubular hydroxyphosphite $Zn_{11}\square(HPO_3)_8(OH)_6$. *Journal of Solid State Chemistry* **107**, 250-257.
- MOORE, P.B. (1973) Bracelets and pinwheels: A topological-geometrical approach to the calcium orthosilicate and alkali sulfate structures. *American Mineralogist* **58**, 32-42.
- MOORE, P. B. & ARAKI, T. (1978a) Angelellite, $Fe_4^{3+}O_3(As^{5+}O_4)_2$: a novel cubic close-packed oxide structure. *Neues Jahrbuch für Mineralogie (Abhandlungen)* **132**, 91-100.
- MOORE, P.B. & ARAKI, T. (1978b) Dumortierite, $Si_3B[Al_{6.75}\square_{0.25}O_{17.25}(OH)_{0.75}]$: a detailed structure analysis. *Neues Jahrbuch für Mineralogie (Abhandlungen)* **132**, 231-241.
- MÜCKE, A. & YOUNESSI, R. (1994) Magnetite-apatite deposits (Kiruna-type) along the Sanandaj-Sirjan zone in the Bafq area, Iran, associated with ultramafic and calcalkaline rocks and carbonatites. *Mineralogy and Petrology* **50**, 219-244.
- NI, Y., LIAO, K., HONG, J., & WEIA, X. (2009) Ni^{2+} ions assisted hydrothermal synthesis of flowerlike $Co_{11}(HPO_3)_8(OH)_6$ superstructures and shape control. *CrystEngComm* **11**, 570-575.
- ONO, A. (1981) Synthesis of dumortierite in the system Al_2O_3 - SiO_2 - B_2O_3 - H_2O . *Journal of the Japanese Association of Mineralogy, Petrology and Economic Geology* **76**, 21-25.

- OZIMA, M., SATO, S., & ZOLTAI, T. (1977) The crystal structure of a lithium-nickel molybdate, $\text{Li}_2\text{Ni}_2\text{Mo}_3\text{O}_{12}$, and the systematics of the structure type. *Acta Crystallographica* **B33**, 2175-2181.
- PEACOR, D.R., ROUSE, R.C., & AHN, J.-H. (1987) Crystal structure of tiptopite, a framework berylllophosphate isotypic with basic cancrinite. *American Mineralogist* **72**, 816-820.
- PECHARSKY, V.K. & ZAVALI, P.Y. (2009) *Fundamentals of Powder diffraction and Structural Characterization of Materials, Second Edition*. DOI: 10.1007/978-0-387-09579-0.
- PEKOV, I.V., OLYSICH, L.V., CHUKANOV, N.V., ZUBKOVA, N.V., PUSHCHAROVSKY, D.YU., VAN, K.V., GIESTER, G., & TILLMANN, E. (2011) Crystal chemistry of cancrinite-group minerals with an AB-type framework: A review and new data. I. Chemical and structural variations. *Canadian Mineralogist* **49**, 1129-1150.
- PEREZ, G., LASSERRE, F., MORET, J., & MAURIN, M. (1976) Structure cristalline des hydroxytellurites de nickel et de cobalt. *Journal of Solid State Chemistry* **17**, 143-149.
- PIECZKA, A. & MARSZALEK, M. (1996) Holtite - the first occurrence in Poland. *Mineralogia Polonica* **27**, 3-8.
- PIECZKA, A., GREW, E. S., GROAT, L. A., & EVANS, R. J. (2011) Holtite and dumortierite from the Szklary pegmatite, Lower Silesia, Poland. *Mineralogical Magazine* **75**, 303-315.
- PIZARRO, J.L., ARRIORTUA, M.I., LEZAMA, L., & ROJO, T. (1993) Synthetic pathways to obtain phosphates and arsenates of Co(II) and Ni(II) related to minerals: magnetic properties. *Solid State Ionics* **63-65**, 71-77.
- PLATONOV, A.N., LANGER, K., CHOPIN, C., ANDRUT, M., & TARAN, M.N. (2000) Fe^{2+} - Ti^{4+} charge-transfer in dumortierite. *European Journal of Mineralogy* **12**, 521-528.
- PLESS, J.D., KIM, H.S., SMIT, J.P., WANG, X., STAIR, P.C., & POEPELMEIER, K.R. (2006) Structure of $\text{Mg}_{2.56}\text{V}_{1.12}\text{W}_{0.88}\text{O}_8$ and vibrational Raman spectra of $\text{Mg}_{2.5}\text{VWO}_8$ and $\text{Mg}_{2.5}\text{VMoO}_8$. *Inorganic Chemistry* **45**, 514-520.
- PRYCE, M.W. (1971) Holtite: a new mineral allied to dumortierite. *Mineralogical Magazine* **38**, 21-25.
- RAADE, G. (1990) Hydrothermal syntheses of $\text{Mg}_2\text{PO}_4\text{OH}$ polymorphs. *Neues Jahrbuch für Mineralogie (Monatshefte)* **1990**, 289-300.
- RAADE, G. & MLADECK, M.H. (1979) Holtedahlite, a new magnesium phosphate from Modum, Norway. *Lithos* **12**, 283-287.
- RAADE, G., RÖMMING, C., & MEDENBACH, O. (1998) Carbonate-substituted phosphoellenbergerite from Modum, Norway: description and crystal structure. *Mineralogy and Petrology* **62**, 89-101.
- ROJO, J.M., MESA, J.L., PIZARRO, J.L., GARCÍA-TOJAL, G., ARRIORTUA, M.I., & ROJO, T. (2002) Hydrothermal synthesis at high pressure and temperature of the $\text{Mg}_{7.5}\text{Ni}_6\text{H}_3(\text{AsO}_4)_8(\text{OH})_6$ and $\text{Mg}_8\text{Ni}_6\text{H}_3(\text{PO}_4)_8(\text{OH})_6$ compounds. *High Pressure Research* **22**, 569-572.
- RÖMMING, C. & RAADE, G. (1989) The crystal structure of natural and synthetic holtedahlite. *Mineralogy and Petrology* **40**, 91-100.
- SCHALLER, W.T. (1905) Dumortierite. *United States Geological Survey, Bulletin* **262**, 91-120.
- SEBASTIAN, L., PIFFARD, Y., SHUKLA, A.K., TAULELLE, F., & GOPALAKRISHNAN, J. (2003) Synthesis, structure and lithium-ion conductivity of $\text{Li}_{2-2x}\text{Mg}_{2+x}(\text{MoO}_4)_3$ and $\text{Li}_3\text{M}(\text{MoO}_4)_3$ ($\text{M}^{\text{III}} = \text{Cr, Fe}$). *Journal of Materials Chemistry* **13**, 1797-1802.
- SEDELLO, O. & MÜLLER-BUSCHBAUM, H. (1996) Synthese und Kristallstruktur von $(\text{Cu, Fe})_{3.63}\text{Mo}_3\text{O}_{12}$. Ein Oxometallat mit eindimensional flächenverknüpften Oktaederketten. *Zeitschrift für Naturforschung B* **51**, 90-94.
- SHANNON, R.D. (1976) Revised effective ionic radii and systematic studies of interatomic distances in halides and chalcogenides. *Acta Crystallographica* **A32**, 751-767.
- SIRBESCU, M. & JENKINS, D.M. (1999) Experiments on the stability of cancrinite in the system $\text{Na}_2\text{O-CaO-Al}_2\text{O}_3\text{-SiO}_2\text{-CO}_2\text{-H}_2\text{O}$. *American Mineralogist* **84**, 1850-1860.
- SMIT, J.P., KIM, H.S., PLESS, J.D., STAIR, P.C., & POEPELMEIER, K.R. (2006b) Probing the vanadyl and molybdenyl bonds in complex vanadomolybdenate structures. *Inorganic Chemistry* **45**, 521-528.
- SMIT, J.P., KIM, H.S., SARATOVSKY, I., STARK, K.B., FITZGERALD, G., ZAJAC, G.W., GAILLARD, J.F., POEPELMEIER, K.R., & STAIR, P.C. (2007) A spectroscopic and computational investigation of the vanadomolybdenate local structure in the lyonsite phase $\text{Mg}_{2.5}\text{VMoO}_8$. *Inorganic Chemistry* **46**, 6556-6564.
- SMIT, J.P., McDONALD, T.M., & POEPELMEIER, K.R. (2008) $\text{Li}_3\text{Ti}_{0.75}(\text{MoO}_4)_3$: a lyonsite-type oxide. *Solid State Sciences* **10**, 396-400.
- SMIT, J.P., STAIR, P.C., & POEPELMEIER, K.R. (2006a) The adaptable lyonsite structure. *Chemistry - A European Journal* **12**, 5944-5953.
- SMITH, G.W. (1960) Crystal structure of orthorhombic cobalt molybdate. *Nature* **188**, 306-308.
- SMITH, J.V. (1988) Topochemistry of zeolites and related materials. 1. Topology and geometry. *Chemical Review* **88**, 149-182.
- SZILLAT, H. & MÜLLER-BUSCHBAUM, H. (1995) Synthese und Kristallstruktur von $(\text{Cu, Zn})_{3.75}\text{Mo}_3\text{O}_{12}$. *Zeitschrift für Naturforschung B* **50**, 247-251.

- TANER, M.F. & MARTIN, R.F. (1993) Significance of dumortierite in an aluminosilicate-rich alteration zone, Louvicourt, Quebec. *Canadian Mineralogist* **31**, 137-146.
- VAGGELLI, G., OLMI, F., MASSI, M., GIUNTINI, L., FEDI, M., FIORA, L., COSSIO, R., & BORGHI, A. (2004) Chemical investigation of coloured minerals in natural stones of commercial interest. *Microchimica Acta* **145**, 249-254.
- VOLOSHIN, A.V., GORDIENKO, V.V., GEL'MAN, YE.M., ZORINA, M.L., YELINA, N.A., KUL'CHITSKAYA, YA.A., MEN'SHIKOV, YU.P., POLEZHAYEVA, L.I., RYZHOVA, R.I., SOKOLOV, P.B., & UTOCHKINA, G.I. (1977) Holtite (first find in the USSR) and its relationship with other tantalum minerals in rare-metal pegmatites. *Novyye Mineraly i Pervyye Nakhodki v SSSR* **106(3)**, 337-347 (in Russian).
- WANG, X., HEIER, K.R., STERN, C.L., & POEPELMEIER, K.R. (1997) Crystal structure of $Zn_{3.77}V_{1.54}Mo_{1.46}O_{12}$ containing ZnO_6 trigonal prisms. *Journal of Alloys and Compounds* **255**, 190-194.
- WANG, X., STERN, C.L., & POEPELMEIER, K.R. (1996) Phase relations in the $MgMoO_4$ - $Mg_3V_2O_8$ system and crystal structure of $Mg_{2.54}V_{1.08}Mo_{0.92}O_8$. *Journal of Alloys and Compounds* **243**, 51-58.
- WANG, X., VANDER GRIEND, D.A., STERN, C.L., & POEPELMEIER, K.R. (2000) Site-specific vanadates $Co_4Fe_{3.33}(VO_4)$ and $Mn_3Fe_4(VO_4)_6$. *Inorganic Chemistry* **39**, 136-140.
- WERDING, G. & SCHREYER, W. (1983) High pressure synthesis of dumortierite (abstract). *Terra Cognita (Journal of the European Union of Geosciences)* **3**, 165 (GD 27).
- WERDING, G. & SCHREYER, W. (1990) Synthetic dumortierite: its PTX-dependent compositional variations in the system Al_2O_3 - B_2O_3 - SiO_2 - H_2O . *Contributions to Mineralogy and Petrology* **105**, 11-24.
- ZHANG F., ZAVALJI, P.Y., & WHITTINGHAM, M.S. (1999) Synthesis and characterization of a pipe-structure manganese vanadium oxide by hydrothermal reaction. *Journal of Materials Chemistry* **9**, 3137-3140.
- ZUBKOVA, N.V., PUSHCHAROVSKY, D.YU., KABALOV, YU.K., KAZANTSEV, S.S., & VOLOSHIN, A.V. (2006) Crystal structure of holtite II. *Crystallography Reports* **51**, 16-22.
- ZUBKOVA, N.V., PUSHCHAROVSKY, D.YU., PASERO, M., CHUKANOV, N.V., & MERLINO, S. (2007) Crystal structure of phosphorus-rich ellenbergerite. *Crystallography Reports* **52**, 199-202.

Submitted May 16, 2012, revised manuscript accepted August 17, 2012.

